Closed-Form CRLBs for SNR Estimation From Turbo-Coded BPSK-, MSK-, and Square-QAM-Modulated Signals

Faouzi Bellili, Achref Methenni, and Sofiène Affes, *Senior Member, IEEE*

***Abstract*—In this contribution, we derive for the first time the closed-form expressions for the Cramér–Rao lower bounds (CRLBs) of the signal-to-noise ratio (SNR) estimates from BPSK-, MSK- and square-QAM modulated signals over turbo-coded transmissions. These CRLBs, relatively easy to derive from BPSK, MSK and QPSK transmissions, become extremely challenging with higher-order square-QAM-modulated signals. In the latter, by exploiting the structure of the Gray mapping, we are able to factorize the likelihood function thereby linearizing all the derivation steps for the Fisher information matrix (FIM) elements. We also propose another approach that allows the evaluation of the considered bounds using extensive Monte Carlo computer simulations. The analytical CRLBs coincide exactly with their empirical counterparts validating thereby our new analytical expressions. Numerical results suggest that the CLRBs for code-aided (CA) SNR estimates range between the CRLBs for non-data-aided (NDA) SNR estimates and those for data-aided (DA) ones, thereby highlighting the expected potential in SNR estimation improvement from the coding gain. Indeed, the CA CRLBs improve by decreasing the overall coding rate due to enhanced decoding capabilities. However they do increase with the modulation order for a given code rate. Finally, the derived bounds are also valid for LDPC coded systems and they can be evaluated when the latter are decoded using the turbo principal.**

***Index Terms*—BPSK, code-aided (CA), Cramér-Rao lower bound (CRLB), data-aided (DA), extrinsic information, gray mapping, lDPC codes, MSK, non-data-aided (NDA), signal-to-noise ratio (SNR), soft decoding, square QAM, turbo codes.**

I. Introduction

MODERN wireless communication systems rely on the *a priori* knowledge of the propagation conditions in order to enhance their capacity. In particular, the SNR is considered as a key parameter whose *a priori* knowledge (estimation) can be exploited at both the receiver and the transmitter (through feedback) in order to reach the desired enhanced/optimal performance by using various adaptive schemes. For instance, the SNR level is a key measure of the channel quality [1] and it is hence required in multiple applications such as equalization [2], [3], adaptive modulation, link adaptation, and power control [4], [5], just to name a few.

Roughly speaking, SNR estimators can be broadly divided into two major categories: i) data-aided (DA) techniques in which the estimation process relies on a perfectly known transmitted sequence, and ii) non-data-aided (NDA) techniques where the estimation process is applied blindly using the received samples only. Most interestingly, the NDA approaches share the advantage of not impinging on the whole throughput of the system (high spectral efficiency). However, they usually exhibit very poor estimation performance in the low-SNR region, especially in the presence of short data records. In such harsh conditions, code-aided (CA) estimation can be envisaged to substantially enhance performance while being spectrally efficient. In this context, turbo codes [6]–[8] have gained considerable attention over the last two decades thanks to their impressive ability to operate in the near-Shannon limit even at very low SNR levels. Therefore, they have been already adopted in many recent and upcoming wireless communication standards such as 4G long-term evolution (LTE), LTE-advanced (LTE-A) and beyond (LTE-B) [9].

Very recently, it has been shown in [14]–[17] that the SNR estimation performance can be substantially enhanced by exploiting some priors[1] that are delivered during the decoding process of the transmitted bits. More specifically, it was shown that CA estimation performs — over a wide range of practical SNRs — nearly the same as in the ideal DA case where all the bits are perfectly known *a priori*. In turbo-coded systems, for instance, CA estimation schemes may rely on the soft information obtained from the soft-input soft-output (SISO) decoder. The optimal SISO algorithm [in the sense of minimum bit error rate (BER)] follows a maximum *a posteriori* (MAP) approach, also known as the BCJR algorithm [18], [19]. Yet, the successful implementation of the MAP decoder itself requires the *a priori* knowledge (i.e., estimation) of the SNR [19]. Therefore, the effect of the SNR mismatch on the performance of turbo-decoding has been the subject of various studies [19]–[24]. It was found, in the particular case of BPSK signals, that over-estimating the

Manuscript received October 07, 2013; revised March 30, 2014 and April 23, 2014; accepted May 01, 2014. Date of publication July 08, 2014; date of current version July 10, 2014. The associate editor coordinating the review of this manuscript and approving it for publication was Prof. Pascal Larzabal. Work supported by the Discovery Grants Program of NSERC and a Discovery Accelerator Supplement (DAS) Award.

The authors are with the INRS-EMT, Montreal, QC H5A 1K6, Canada (e-mail: bellili@emt.inrs.ca; methenni@emt.inrs.ca; affes@emt.inrs.ca).

Color versions of one or more of the figures in this paper are available online at http://ieeexplore.ieee.org.

Digital Object Identifier 10.1109/TSP.2014.2328328

[1]In code-aided estimation schemes, the transmitted symbols are also completely unknown. Yet, much information about these symbols can be acquired during the iterative decoding of the transmitted bits. This information is then exploited in the estimation process as *a priori* knowledge.

SNR by several dBs can be tolerated while insuring acceptable BER performance. In contrast, under-estimation by more than 2 dB leads to significant decoding errors.

In order to satisfy the increasing demand for very high-data rate communications, higher-order modulations are also a key feature of current and future standards (LTE, LTE-A and LTE-B) [25]. In presence of higher-order-modulated signals, the effect of SNR mismatch was also investigated in [23] and found to be remarkably different and more influential on performance. Indeed, the estimated SNR plays a different role in the calculation of the bit metric for each modulation scheme, thereby leading to different decoding performance. The performance of turbo-coded systems transmitting higher-order-modulated signals is typically more sensitive to SNR over-estimation [23].

From the algorithmic point of view, many NDA SNR estimators suitable for QAM signals have been recently introduced in [10]–[13]. Many SNR estimators suited for turbo-coded systems have been also introduced in the open literature [14]–[17]. The performance of such estimators is usually assessed in terms of error variance; yet it still requires to be gaged against an absolute benchmark. The Cramér-Rao lower bound (CRLB), a well known fundamental bound [26] in estimation theory, meets this requirement since it sets the minimum achievable variance for all the unbiased estimators. Unlike other loose bounds, the *stochastic* [2] CRLB is known to be achieved, asymptotically, by the stochastic maximum likelihood estimator. Yet, even in the case of uncoded transmissions, the complex structure of the likelihood function makes it extremely hard, if not impossible, to derive analytical expressions for such bounds, especially for higher-order modulations. Therefore, they are usually evaluated empirically, for both non-coded and coded systems.

More than a decade ago, the first SNR CRLBs in closed-form expressions were derived in the DA scenario [27] for different modulations types and orders. In the same work, they were likewise obtained in the NDA case only for BPSK and QPSK modulations. This was followed by the investigations in [28], [29] by finding a way out of the long-lasting impasse standing between the very first set of analytical results in [27] and their generalization to arbitrary higher-order square-QAM modulations due to the increasingly inextricable form of the likelihood function. Obviously, the latter is expected to become even more complicated in CA transmissions, thereby revealing unambiguously the extreme challenge and value of this work's clearly-stated objective when properly positioned in the current state of the art. A compelling illustration of the literature limitation persisting so far is that CA SNR estimators have been very often compared in performance to the DA CRLBs (as recently done in [17] and [20]). The latter might offer an accurate benchmark for BPSK signals, but become excessively optimistic[3] in the presence of higher-order-modulated signals, especially at low SNR values (see Section V for more details). So far, the CRLBs for code-aware (CA) SNR estimation have been derived analytically only in the very basic case of BPSK-modulated signals [14]. It is also worth mentioning that some closed-form expressions for coded large QAM phase CRLBs have recently been reported in [30], [31] which show clearly the advantage of CA estimation over NDA estimation.

Motivated by all the aforementioned facts, we derive in this paper, for the first time, the analytical expressions for the CA CRLBs of SNR estimates from coded BPSK-, MSK- and arbitrary square-QAM-modulated signals. For the sole purpose of their validation, we also derive their empirical counterparts. The latter could have stood as valuable contributions by themselves in this topic's typical literature (cf. successive milestone extensions of the NDA CRLBs for the QAM signals from BPSK/QPSK [32]–[36], all derived empirically though in [37]–[42] within about a decade period between [27] and [28], [29]) if they were not made obsolete by this work's contributions even before inception. Numerical results will show, indeed, that the new analytical CRLBs coincide with their empirical values. They will also reveal that the CA scheme lies between the NDA and DA schemes in terms of CRLB performance limit, acting therefore as its upper and lower ends, respectively. The CA's performance bound moves up or down to either ends with the coding rate relatively increasing or decreasing, respectively. Furthermore, all three CRLBs tend to coincide at higher SNR values or lower modulation orders.

The rest of this paper is organized as follows. In Section II, we introduce the system model. In Section III, we derive the explicit expression for the log-likelihood function (LLF) for different transmissions. In Section IV, we derive new analytical expressions for the corresponding CRLBs and we propose, as well, another approach that allows the evaluation of the considered bounds empirically. In Section V, we present and discuss the simulation results of the newly derived bounds. Finally, we draw out some concluding remarks in Section VI.

In the following, vectors and matrices will be represented in lower- and upper-case bold fonts, respectively. Moreover, $\{.\}^T$ and $\{.\}^H$ will denote the transpose and the Hermitian (transpose conjugate) operators, respectively. The operators $\Re\{.\}$ and $\Im\{.\}$ will return, respectively, the real and imaginary parts of any complex number whereas $\{.\}^*$ and $|.|$ will return its conjugate and its amplitude, respectively. We will denote by j the pure complex number that verifies $j^2 = -1$. We will also denote the probability mass function (PMF) for discrete random variables by $P[.]$ and the probability density function (pdf) for continuous random variables by $p[.]$.

II. System Model

Consider a turbo-coded system where a binary sequence of information bits (grouped into consecutive blocks containing Q bits each) is fed into a turbo encoder, of rate R. The encoder consists of two identical recursive and systematic convolutional codes (RSCs) with generator polynomials $[g1,\ g2]$. The two RSCs are concatenated in parallel via an interleaver of size L. The coded bits are then fed into a puncturer which selects an appropriate combination of the parity bits, from both encoders, in order to achieve the desired overall rate R. Each block of Q

[2]The stochastic designation is usually adopted to refer to the case of unknown and random transmitted symbols. This is in contrast with the *deterministic* CRLB where the symbols are unknown but deterministic.

[3]The DA CRLBs are indeed the same for all linearly-modulated signals [27], i.e., they would misleadingly suggest the same bound regardless of the modulation type or order if taken as a benchmark when it is in fact different in CA transmissions.

coded bits (systematic and parity bits) is scrambled with an outer interleaver, and then mapped onto any Gray-coded constellation[4]. Finally, the obtained symbols are transmitted over the wireless channel. The received signal is sampled at the output of the matched filter. Then by assuming *imperfect* phase and frequency synchronization, the observed samples are modeled as follows:

$$y(k) = S\, x(k) e^{j(2\pi k\vartheta+\phi)} + w(k), \quad k = 0, 1, 2, \ldots, K-1, \tag{1}$$

where, at time index k, $x(k)$ is the k^{th} coded symbol that is transmitted over the wireless channel and $y(k)$ is its corresponding received sample. The channel is assumed to be slowly time-varying, over the entire observation window of size K, and hence of constant but unknown gain, S, and phase shift ϕ. The parameter ϑ stands for the normalized carrier frequency offset (CFO) stemming from Doppler effects and/or synchronization errors between the transmitter's and receiver's local oscillators. The noise components, $w(k)$, are modeled by a zero-mean complex circular Gaussian random variable, with independent real and imaginary parts, each of variance σ^2 (i.e., of total noise power $N_0 = 2\sigma^2$). Without loss of generality, we further assume that the energy of the transmitted symbols is normalized[5] to one, i.e., $\mathrm{E}\{|x(k)|^2\} = 1$. Using the K observations, $\{y(k)\}_{k=0}^{K-1}$, the true SNR, ρ, that we wish to estimate is defined as:

$$\rho = \frac{\mathrm{E}\{S^2|x(k)|^2\}}{2\sigma^2} = \frac{S^2}{2\sigma^2}. \tag{2}$$

From (2), it is seen that there are two unknown parameters which are involved in the derivation of the SNR CRLBs, namely S and σ^2. Therefore, it is mathematically more convenient to gather them into a single parameter vector $\boldsymbol{\alpha} = [S \quad \sigma^2]$. Depending on the SNR scale (i.e., the SNR in the *decibels* [dB] or *linear* scale), we define the following transformations:

$$g(\boldsymbol{\alpha}) = \begin{cases} 10\log_{10}\left(S^2/2\sigma^2\right) & \text{(in [dB] scale)} \\ S^2/2\sigma^2 & \text{(in linear scale)} \end{cases} \tag{3}$$

For mathematical convenience, as well, we gather all the recorded data samples in a single vector:

$$\boldsymbol{y} = [y(0), y(1), \ldots, y(K-1)]^T. \tag{4}$$

The LLF of the system will be denoted as $L_{\boldsymbol{y}}(\boldsymbol{\alpha}) = \ln\left(p[\boldsymbol{y};\boldsymbol{\alpha}]\right)$ where $p[\boldsymbol{y};\boldsymbol{\alpha}]$ is the pdf of the received vector $\boldsymbol{y}$ parameterized by the unknown parameter vector $\boldsymbol{\alpha}$. As shown in [26], the CRLB for the parameter transformation in (3) is given by:

$$\mathrm{CRLB}(\rho) = \frac{\partial g(\boldsymbol{\alpha})}{\partial \boldsymbol{\alpha}} \boldsymbol{I}^{-1}(\boldsymbol{\alpha}) \frac{\partial g(\boldsymbol{\alpha})}{\partial \boldsymbol{\alpha}}^T, \tag{5}$$

[4]As mentioned previously, we shall later restrict ourselves to BPSK, MSK and square-QAM constellations only.

[5]If the transmit energy, P, is not unitary, it can be easily incorporated as an unknown scaling factor into the channel coefficient by estimating $\tilde{S} = \sqrt{P}S$ instead of S in (1).

where the derivative, $\partial g(\boldsymbol{\alpha})/\partial\boldsymbol{\alpha}$, is given by:

$$\frac{\partial g(\boldsymbol{\alpha})}{\partial \boldsymbol{\alpha}} = \begin{cases} \left[\frac{20}{\ln(10)S} \quad \frac{-10}{\ln(10)\sigma^2}\right] & \text{(in [dB] scale)} \\ \left[\frac{S}{\sigma^2} \quad -\frac{S^2}{2\sigma^4}\right] & \text{(in linear scale)} \end{cases} \tag{6}$$

and $\boldsymbol{I}(\boldsymbol{\alpha})$ is the Fisher information matrix (FIM) defined as:

$$[\boldsymbol{I}(\boldsymbol{\alpha})]_{i,l} = -\mathrm{E}\left\{\frac{\partial^2 L_{\boldsymbol{y}}(\boldsymbol{\alpha})}{\partial\alpha_i \partial\alpha_l}\right\} \quad i,l = 1,2. \tag{7}$$

In (7), $\{\alpha_i\}_{i=1,2}$ are the elements of the unknown parameter vector $\boldsymbol{\alpha}$. Usually, the analytical derivation of the stochastic CRLB involves tedious algebraic manipulations. These consist in three major steps: 1) derivation of the log-likelihood function (LLF), 2) derivation of the FIM elements, and then 3) derivation of the CRLB expression using (5). In the sequel, these three steps will be accomplished in the given order.

III. Derivation of the LLF

To begin with, we assume that the symbols are drawn from any M-ary constellation. This is because, as will be seen shortly, the first derivation steps are valid for linearly-modulated signals in general. However, later on, we will restrict ourselves to BPSK, MSK and square-QAM constellations for reasons that will become apparent by then. We assume the constellation to be Gray-coded and denote its alphabet by $\mathcal{C} = \{c_0, c_1, \ldots, c_{M-1}\}$. Moreover, we will — from now on — adopt the two following notations:

$$c_m \longleftrightarrow \bar{b}_1^m \bar{b}_2^m \cdots \bar{b}_{\log_2(M)}^m, \;\; x(k) \longleftrightarrow b_1^k b_2^k \cdots b_{\log_2(M)}^k, \tag{8}$$

to designate the mapping between the m^{th} constellation point c_m [respectively, the k^{th} transmitted symbol $x(k)$] and its associated Gray-coded bits [respectively, the k^{th} block of conveyed bits]. Due to the large-size interleaver, the coded bits can be assumed as statistically independent. This assumption is indeed pervasive in code-aided estimation [15], [43], [44], [46]. Consequently, the transmitted symbols (which are *soft* representations for different blocks of such independent bits) can also be considered as independent thereby yielding:

$$p[\boldsymbol{y};\boldsymbol{\alpha}] = \prod_{k=0}^{K-1} p[y(k);\boldsymbol{\alpha}], \tag{9}$$

where $p[y(k);\boldsymbol{\alpha}]$ is the pdf of the individual received sample, $y(k)$, which is given by:

$$\begin{aligned} p[y(k);\boldsymbol{\alpha}] &= \sum_{c_m\in\mathcal{C}} P[x(k)=c_m]\, p[y(k)|x(k)=c_m;\boldsymbol{\alpha}], \\ &= \sum_{m=0}^{M-1} \frac{P[x(k)=c_m]}{2\pi\sigma^2} \exp\left\{-\frac{|y(k)-S_{\phi,\vartheta}\, c_m|^2}{2\sigma^2}\right\}, \end{aligned} \tag{10}$$

in which we use the notation $S_{\phi,\vartheta} = Se^{j(2\pi k\vartheta+\phi)}$. Now, in the case of higher-order modulations where each constellation point represents more that one bit (i.e., $\log_2(M) > 1$), and again, due

to the independence of the coded bits, the probability of each transmitted symbol, $x(k)$, is factorized into the probabilities of the elementary bits it conveys:

$$P[x(k)=c_m] = P\left[b_1^k=\bar{b}_1^m, b_2^k=\bar{b}_2^m, \ldots, b_{\log_2(M)}^k=\bar{b}_{\log_2(M)}^m\right] = \prod_{l=1}^{\log_2(M)} P\left[b_l^k=\bar{b}_l^m\right]. \quad (11)$$

We also define the so-called log-likelihood ratio (LLR) of each transmitted bit, b_l^k, as follows:

$$L_l(k) = \ln\left(\frac{P[b_l^k=1]}{P[b_l^k=0]}\right). \quad (12)$$

Then, using (12) and the fact that $P[b_l^k=0]+P[b_l^k=1]=1$, the *a priori* probabilities of the transmitted coded bits can be expressed as:

$$P[b_l^k=1]=\frac{e^{L_l(k)/2}}{2\cosh\left(L_l(k)/2\right)},\ P[b_l^k=0]=\frac{e^{-L_l(k)/2}}{2\cosh\left(L_l(k)/2\right)}. \quad (13)$$

A. LLF for BPSK and MSK Signals

In BPSK transmissions, the constellation alphabet is simply given by $\mathcal{C} = \{+1,-1\}$. In MSK transmissions, however, the transmitted symbols are constructed recursively as $a_{k+1}=ja_k(2b_k-1)$ where b_k is the sequence of coded bits and a_0 is the original value drawn from the set $\{-1,-j,+1,+j\}$. The pdf of the received vector $\boldsymbol{y}$ parameterized by $\boldsymbol{\alpha}$ is expressed as follows:

$$p[\boldsymbol{y};\boldsymbol{\alpha}] = \prod_{k=0}^{K-1}\left(\frac{P[x(k)=d_k]}{2\pi\sigma^2}\exp\left\{-\frac{|y(k)-d_kS_{\phi,\vartheta}|^2}{2\sigma^2}\right\} + \frac{P[x(k)=-d_k]}{2\pi\sigma^2}\exp\left\{-\frac{|y(k)+d_kS_{\phi,\vartheta}|^2}{2\sigma^2}\right\}\right), \quad (14)$$

where d_k is given by $d_k = 1$ for BPSK and $d_k = j^{k-1}a_0$ for MSK. In addition, in BPSK and MSK transmissions, each transmitted symbol conveys only one bit and, therefore, they both have the same probabilities from the statistical point of view. That is to say: $P[x(k)=1]=P[b_k=1], P[x(k)=-1]=P[b_k=0]$ for BPSK and $P[x(k)=j^{k-1}a_0]=P[b_k=1]$, $P[x(k)=-j^{k-1}a_0]=P[b_k=0]$ for MSK. These *a priori* probabilities are obtained from the LLRs of the transmitted bits — denoted here as $L(k)$ by dropping the subscript l — as follows:

$$P[b_k=1]=\frac{e^{L(k)/2}}{2\cosh\left(L(k)/2\right)},\ P[b_k=0]=\frac{e^{-L(k)/2}}{2\cosh\left(L(k)/2\right)}. \quad (15)$$

Using these results in (14) and after some algebraic manipulations, it can be shown that the LLF of interest[6], $L_{\boldsymbol{y}}(\boldsymbol{\alpha}) = \ln(p[\boldsymbol{y};\boldsymbol{\alpha}])$, is expressed as follows:

$$L_{\boldsymbol{y}}(\boldsymbol{\alpha}) = -K\ln(\sigma^2) - \frac{KS^2}{2\sigma^2} - \frac{1}{2\sigma^2}\sum_{k=0}^{K-1}|y(k)|^2 + \sum_{k=0}^{K-1}\ln\left(\cosh\left(\frac{\Re(y(k)^*d_kS_{\phi,\vartheta})}{\sigma^2}+\frac{L(k)}{2}\right)\right). \quad (16)$$

[6]After dropping the two constant terms $K\ln(2\pi)$ and $\sum_{k=0}^{K-1}\ln\left(2\cosh(L(k)/2)\right)$ which do not depend on the unknown parameters S and σ^2.

B. LLF for QPSK Signals

Here, each transmitted symbol carries two bits. Hence, the constellation alphabet consists of four different symbols, i.e., $\mathcal{C} = \{c_0,c_1,c_2,c_3\}$. Consequently, the pdf of the received sample, $y(k)$, is obtained from (10) as:

$$p[y(k);\boldsymbol{\alpha}] = \sum_{m=0}^{3}\frac{P[x(k)=c_m]}{2\pi\sigma^2}\exp\left\{-\frac{|y(k)-S_{\phi,\vartheta}\,c_m|^2}{2\sigma^2}\right\}. \quad (17)$$

Without loss of generality, we will make the two following assumptions:

- *A1*) The constellation is Gray-coded according to the following mapping: $c_0 \longleftrightarrow 11$, $c_1 \longleftrightarrow 00$, $c_2 \longleftrightarrow 01$ and $c_3 \longleftrightarrow 10$.
- *A2*) $c_0=(1+j)/\sqrt{2}$, $c_1=-c_0$, $c_2=c_0^*$ and $c_3=-c_0^*$.

Therefore, by defining $Q_l(k) \triangleq 1/[2\cosh(L_l(k)/2)]$ for $l = 1,\ 2$, then plugging (13) in (11) and using assumption *A1)*, we obtain:

$$P[x(k)=c_0] = Q_1(k)Q_2(k)e^{\frac{L_1(k)+L_2(k)}{2}}, \quad (18)$$

$$P[x(k)=c_1] = Q_1(k)Q_2(k)e^{-\frac{L_1(k)+L_2(k)}{2}}, \quad (19)$$

$$P[x(k)=c_2] = Q_1(k)Q_2(k)e^{\frac{-L_1(k)+L_2(k)}{2}}, \quad (20)$$

$$P[x(k)=c_3] = Q_1(k)Q_2(k)e^{\frac{L_1(k)-L_2(k)}{2}}. \quad (21)$$

Now, by plugging (18) to (21) back into (17) and using assumption *A2)*, we show after some relatively tedious algebraic manipulations that:

$$p[y(k);\boldsymbol{\alpha}] = \frac{1}{2\pi\sigma^2}\exp\left\{-\frac{S^2+|y(k)|^2}{2\sigma^2}\right\} \times Q_1(k)\cosh\left(\frac{\Re\{y(k)^*S_{\phi,\vartheta}\}}{\sqrt{2}\sigma^2}+\frac{L_2(k)}{2}\right) \times Q_2(k)\cosh\left(\frac{\Im\{y(k)^*S_{\phi,\vartheta}\}}{\sqrt{2}\sigma^2}-\frac{L_1(k)}{2}\right). \quad (22)$$

Thus, the pdf of the received vector, $\boldsymbol{y}$, is factorized as follows:

$$p[\boldsymbol{y};\boldsymbol{\alpha}] = C_{\boldsymbol{y}}(\boldsymbol{\alpha})\prod_{k=0}^{K-1}Q_1(k)\cosh\left(\frac{\Re(y(k)^*S_{\phi,\vartheta})}{\sqrt{2}\sigma^2}+\frac{L_2(k)}{2}\right) \times \prod_{k=0}^{K-1}Q_2(k)\cosh\left(\frac{\Im(y(k)^*S_{\phi,\vartheta})}{\sqrt{2}\sigma^2}-\frac{L_1(k)}{2}\right), \quad (23)$$

where

$$C_{\boldsymbol{y}}(\boldsymbol{\alpha}) = \frac{1}{\sigma^{2K}(2\pi)^K}\exp\left\{-\frac{KS^2}{2\sigma^2}-\frac{1}{2\sigma^2}\sum_{k=0}^{K-1}|y(k)|^2\right\}. \quad (24)$$

By taking the logarithm of (23) and dropping the constant terms involving $Q_1(k)$ and $Q_2(k)$ (which do not depend on S and σ^2), the LLF for QPSK signals develops as follows:

$$L_{\boldsymbol{y}}(\boldsymbol{\alpha}) = -K\ln(\sigma^2) - \frac{KS^2}{2\sigma^2} - \frac{1}{2\sigma^2}\sum_{k=0}^{K-1}|y(k)|^2 + \sum_{k=0}^{K-1}\ln\left(\cosh\left(\frac{\Re\{y(k)^*S_{\phi,\vartheta}\}}{\sqrt{2}\sigma^2}+\frac{L_2(k)}{2}\right)\right) + \sum_{k=0}^{K-1}\ln\left(\cosh\left(\frac{\Im\{y(k)^*S_{\phi,\vartheta}\}}{\sqrt{2}\sigma^2}-\frac{L_1(k)}{2}\right)\right). \quad (25)$$

C. LLF for Square-QAM Signals

To simplify the notations, we will use the two definitions $I(k) \triangleq \Re\{y(k)\}$ and $Q(k) \triangleq \Im\{y(k)\}$ to refer to the inphase and quadrature components of the received samples, respectively. Then, in the presence of arbitrary M-ary QAM-modulated signals, it can be shown that the pdf in (10) can be rewritten as follows:

$$p[y(k);\boldsymbol{\alpha}] = \frac{1}{2\pi\sigma^2}\exp\left\{-\frac{I(k)^2+Q(k)^2}{2\sigma^2}\right\} D_{\boldsymbol{\alpha}}(k), \quad (26)$$

in which

$$D_{\boldsymbol{\alpha}}(k) = \sum_{m=1}^{M} P[x(k)=c_m] e^{-\frac{S^2|c_m|^2}{2\sigma^2}} \exp\left\{\frac{\Re\{c_m y(k)^* S_{\phi,\vartheta}\}}{\sigma^2}\right\}. \quad (27)$$

Hence, the LLF of the system which follows from the logarithm of (9) as $L_{\boldsymbol{y}}(\boldsymbol{\alpha}) = \sum_{k=0}^{K-1} \ln(p[y(k);\boldsymbol{\alpha}])$, develops into:

$$L_{\boldsymbol{y}}(\boldsymbol{\alpha}) = -K\ln\left(2\pi\sigma^2\right) - \frac{1}{2\sigma^2}\sum_{k=0}^{K-1}\left[I(k)^2+Q(k)^2\right] + \sum_{k=0}^{K-1}\ln\left(D_{\boldsymbol{\alpha}}(k)\right). \quad (28)$$

At this stage, it is still very tedious to derive analytical expressions for the considered CRLBs without further manipulating the term $D_{\boldsymbol{\alpha}}(k)$ defined in (27). Actually, considering the special case of square-QAM-modulated signals (i.e., 16–, 64–, and 256–QAM, etc.), and by exploring the structure of the Gray mapping mechanism, we are able to factorize $D_{\boldsymbol{\alpha}}(k)$ into the product of two analogous terms. In fact, when $M = 2^{2p}$ for any integer $p \geq 2$ (i.e., square-QAM constellations), we have $\mathcal{C}_p = \{\pm(2i-1)d_p \pm j(2n-1)d_p\}_{i,n=1,2,\ldots,2^{p-1}}$, where $2d_p$ is the intersymbol distance in the I/Q plane. Note here that from now on the constellation alphabet will be indexed by the integer p that defines the modulation order (i.e., $\mathcal{C} = \mathcal{C}_p$). The square-QAM constellation energy is supposed to be normalized to one:

$$\frac{\sum_{m=1}^{2^{2p}}|c_m|^2}{2^{2p}} = 1, \quad (29)$$

from which the expression of d_p is obtained as follows:

$$d_p = \frac{2^{p-1}}{\sqrt{2^p\sum_{m=1}^{2^{p-1}}(2m-1)^2}}. \quad (30)$$

Now, by denoting $\tilde{\mathcal{C}}_p = \{(2i-1)d_p + j(2n-1)d_p\}_{i,n=1}^{2^{p-1}}$ the subset of the alphabet that consists of the points which lie in the top-right quadrant of the constellation, one can write $\mathcal{C}_p = \tilde{\mathcal{C}}_p \cup (-\tilde{\mathcal{C}}_p) \cup \tilde{\mathcal{C}}_p^* \cup (-\tilde{\mathcal{C}}_p^*)$. Therefore (27) can be expressed as follows:

$$\begin{aligned} D_{\boldsymbol{\alpha}}(k) = \sum_{\tilde{c}_m\in\tilde{\mathcal{C}}_p} \exp\left\{-\frac{S^2|\tilde{c}_m|^2}{2\sigma^2}\right\} \\ \times\Bigg(P[x(k)=\tilde{c}_m]\exp\left\{\frac{\Re\{\tilde{c}_m y^*(k)S_{\phi,\vartheta}\}}{\sigma^2}\right\} \\ + P[x(k)=-\tilde{c}_m]\exp\left\{\frac{\Re\{-\tilde{c}_m y^*(k)S_{\phi,\vartheta}\}}{\sigma^2}\right\} \\ + P[x(k)=\tilde{c}_m^*]\exp\left\{\frac{\Re\{\tilde{c}_m^* y^*(k)S_{\phi,\vartheta}\}}{\sigma^2}\right\} \\ + P[x(k)=-\tilde{c}_m^*]\exp\left\{\frac{\Re\{-\tilde{c}_m^* y^*(k)S_{\phi,\vartheta}\}}{\sigma^2}\right\}\Bigg). \end{aligned} \quad (31)$$

Another important detail that must be addressed, in order to further simplify the term $D_{\boldsymbol{\alpha}}(k)$, is the Gray mapping scheme of the constellation. Indeed, we will show through a simple Gray coding mechanism how this structure can be used to factorize $D_{\boldsymbol{\alpha}}(k)$, linearizing thereby the LLF expression in (28). The procedure applies in the same way to all possible Gray mapping schemes, yet the obtained final CRLB expressions will still hold the same. First, combining the two results in (13) and assuming that the symbol c_m is transmitted during the k^{th} time instant (i.e., $x(k) = c_m$), we obtain the following generic formula for the *a priori* probability of each conveyed bit:

$$P[b_l^k = \bar{b}_l^m] = \frac{e^{(2\bar{b}_l^m-1)\frac{L_l(k)}{2}}}{2\cosh\left(\frac{L_l(k)}{2}\right)}, \quad (32)$$

where $\bar{b}_l^m$ can be 0 or 1. Therefore, recalling that $\log_2(M) = 2p$ (for square-QAM constellations) and injecting (32) in (11), the symbol probabilities $P[x(k)=c_m]$ are given by:

$$P[x(k)=c_m] = \underbrace{\left(\prod_{l=1}^{2p}\frac{1}{2\cosh\left(L_l(k)/2\right)}\right)}_{\beta_k}\prod_{l=1}^{2p} e^{(2\bar{b}_l^m-1)\frac{L_l(k)}{2}}. \quad (33)$$

Next, we describe a simple process for the recursive construction of any Gray-coded square-QAM constellation. Some hidden properties of such constellations will be revealed — from this recursive process — and carefully exploited in order to factorize the term $D_{\boldsymbol{\alpha}}(k)$ in (31). In fact, starting from any basic QPSK constellation and a given $2^{2(p-1)}$-QAM Gray-coded constellation, it is possible to build a 2^{2p}-QAM Gray-coded one as follows:

- *step 1*: build the top right quadrant of the desired 2^{2p}-QAM constellation from all the points[7] of the available $2^{2(p-1)}$-QAM constellation.
- *step 2*: build the three remaining quadrants of the new 2^{2p}-QAM constellation by symmetries on: i) the x-axis to obtain the bottom-right quadrant, ii) the y-axis to obtain the top-left quadrant; and iii) the center point to obtain the bottom-left quadrant. Yet, the points of the orig-

[7]The same points' layout in the original $2^{2(p-1)}$-QAM constellation is used, i.e., the constellation is placed as is in the new quadrant.

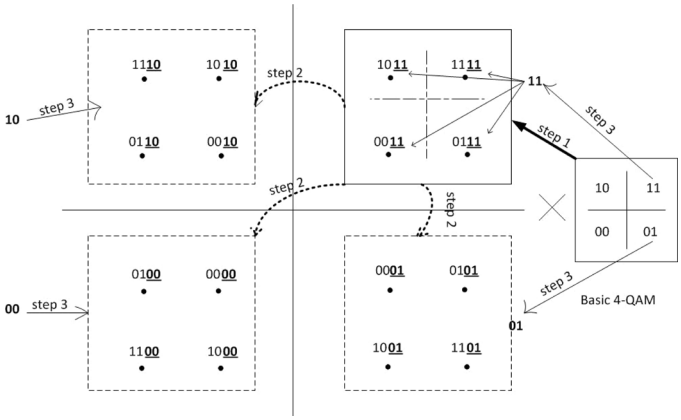

Fig. 1. Recursive construction of Gray-coded square-QAM constellations illustrated here from 4-QAM to 16-QAM.

inal $2^{2(p-1)}$-QAM constellation represent each $2(p-1)$ bits only. Therefore, two bits are still missing in each point of the new 2^{2p}-QAM constellation that must represent $2p$ bits.

- *step 3*: copy the two missing bits from each quadrant of a basic Gray-coded QPSK constellation to all the points that belong to the same quadrant of the new constellation. Without loss of generality, we will use as a basic QPSK constellation the one defined by assumptions *A1)* and *A2)* in Section III-B [just after (17)].

As one example given in Fig. 1, we illustrate the recursive construction of a Gray-coded 16-QAM constellation from a 4-QAM Gray-coded one. Just as depicted in this figure and again without loss of generality, we will use in the sequel the following assumption: *A3)* the two bits added in "*step 3*" occupy the two least significant positions in each symbol of the new 2^{2p}-QAM constellation.

To see how the three steps ("*step 1*" to "*step 3*") allow the construction of any Gray-coded square-QAM constellation, two relevant remarks are in order: i) the basic Gray-coded QPSK constellation can be rotated by modifying the mapping of assumption *A1)*, and ii) assumption *A3)* can also be modified by placing the two missing bits of "*step 3*" at any two positions, i.e., neither being necessarily consecutive nor being the two least significant bits (LSBs) [as considered in assumption *A3)* for the sole sake of clarity].

Due to symmetries in "*step 2*", each four symbols $\tilde{c}_m$, $\tilde{c}_m^*$, $-\tilde{c}_m$ and $-\tilde{c}_m^*$ have the same $2(p-1)$ most significant bits (MSBs), $\bar{b}_1^m \bar{b}_2^m \bar{b}_3^m \ldots \bar{b}_{2p-3}^m \bar{b}_{2p-2}^m$, for any symbol $\tilde{c}_m$ ($m = 1, 2, \ldots, 2^{2(p-1)}$) lying in the top-right quadrant ($\tilde{\mathcal{C}}_p$) of the new 2^{2p}-QAM constellation. Thus, if we consider these $2(p-1)$ MSBs alone and define:

$$\mu_{k,p}(c_m) \triangleq \prod_{l=1}^{2p-2} e^{(2\bar{b}_l^m - 1)\frac{L_l(k)}{2}}, \quad \forall c_m \in \mathcal{C}_p, \tag{34}$$

we can then immediately see that:

$$\mu_{k,p}(\tilde{c}_m) = \mu_{k,p}(-\tilde{c}_m) = \mu_{k,p}(\tilde{c}_m^*) = \mu_{k,p}(-\tilde{c}_m^*), \ \forall \tilde{c}_m \in \tilde{\mathcal{C}}_p. \tag{35}$$

As seen from the right-hand side of (34), it is worth mentioning here that $\mu_{k,p}(c_m)$ is not defined for $p = 1$, i.e., for QPSK constellations. We extend its definition for the latter simply by taking $\mu_{k,1}(c_m) = 1 \ \forall \ c_m \in \mathcal{C}_1$. It will be seen later that this choice is consistent with all the derivations. Then, by focusing on the two remaining LSBs ($\bar{b}_{2p-1}^m$ and $\bar{b}_{2p}^m$) and recalling the Gray mapping of the basic QPSK constellation [depicted in Fig. 1, cf. assumptions *A1)* and *A2)*], it follows that:

$$\bar{b}_{2p-1}^m \bar{b}_{2p}^m = \begin{cases} 11 & \forall \ \tilde{c}_m \in \tilde{\mathcal{C}}_p \\ 00 & \forall -\tilde{c}_m \in -\tilde{\mathcal{C}}_p \\ 01 & \forall \ \tilde{c}_m^* \in \tilde{\mathcal{C}}_p^* \\ 10 & \forall -\tilde{c}_m^* \in -\tilde{\mathcal{C}}_p^*. \end{cases} \tag{36}$$

Of course, these intermediate results change according to the specific choice of the basic QPSK constellation involved in "*step 3*". Consequently, one might wonder how the final results could still stand valid for all possible Gray mapping schemes of the underlying 2^{2p}-QAM constellation. Actually, in this paper, $\tilde{\mathcal{C}}_p$ is defined to be the top-right quadrant of this constellation simply because, according to assumption *A1)*, the two bits "11" are placed in the top-right quadrant of the basic QPSK constellation. Therefore, exactly the same derivation steps can be conducted by defining $\tilde{\mathcal{C}}_p$ to be the quadrant that corresponds to the bits "11" in any other basic QPSK constellation and then decomposing the whole alphabet similarly, i.e., $\mathcal{C}_p = \tilde{\mathcal{C}}_p \cup (-\tilde{\mathcal{C}}_p) \cup \tilde{\mathcal{C}}_p^* \cup (-\tilde{\mathcal{C}}_p^*)$.

Now, upon using (35) and (36) in (33), it follows that for any $\tilde{c}_m \in \tilde{\mathcal{C}}_p$, we have:

$$P[x(k) = \tilde{c}_m] = \beta_k \ \mu_{k,p}(\tilde{c}_m) \ e^{\frac{L_{2p-1}(k)}{2}} e^{\frac{L_{2p}(k)}{2}}, \tag{37}$$

$$P[x(k) = \tilde{c}_m^*] = \beta_k \ \mu_{k,p}(\tilde{c}_m) \ e^{-\frac{L_{2p-1}(k)}{2}} e^{\frac{L_{2p}(k)}{2}}, \tag{38}$$

$$P[x(k) = -\tilde{c}_m] = \beta_k \ \mu_{k,p}(\tilde{c}_m) \ e^{-\frac{L_{2p-1}(k)}{2}} e^{-\frac{L_{2p}(k)}{2}}, \tag{39}$$

$$P[x(k) = -\tilde{c}_m^*] = \beta_k \ \mu_{k,p}(\tilde{c}_m) \ e^{\frac{L_{2p-1}(k)}{2}} e^{-\frac{L_{2p}(k)}{2}}. \tag{40}$$

Therefore, plugging these probabilities back into (31) and using the identity $e^x + e^{-x} = 2\cosh(x)$, it can be shown that:

$$\begin{aligned} & D_{\boldsymbol{\alpha}}(k) \\ & = 2\beta_k \sum_{\tilde{c}_m \in \tilde{\mathcal{C}}_p} \exp\left\{-\frac{S^2|\tilde{c}_m|^2}{2\sigma^2}\right\} \mu_{k,p}(\tilde{c}_m) \\ & \quad \times \left[\cosh\left(\frac{\Re\{\tilde{c}_m \, y^*(k) S_{\phi,\vartheta}\}}{\sigma^2} + \frac{L_{2p-1}(k)}{2} + \frac{L_{2p}(k)}{2}\right)\right. \\ & \quad \left. + \cosh\left(\frac{\Re\{\tilde{c}_m^* \, y^*(k) S_{\phi,\vartheta}\}}{\sigma^2} - \frac{L_{2p-1}(k)}{2} + \frac{L_{2p}(k)}{2}\right)\right]. \end{aligned} \tag{41}$$

Furthermore, using the relationship $\cosh(x) + \cosh(y) = 2\cosh\left(\frac{x+y}{2}\right)\cosh\left(\frac{x-y}{2}\right)$ along with the two identities $\tilde{c}_m + \tilde{c}_m^* = 2\Re\{\tilde{c}_m\}$ and $\tilde{c}_m - \tilde{c}_m^* = 2j\Im\{\tilde{c}_m\}$, (41) is rewritten as follows:

$$\begin{aligned} & D_{\boldsymbol{\alpha}}(k) \\ & = 4\beta_k \sum_{\tilde{c_m} \in \tilde{\mathcal{C}}_p} \left[\exp\left\{-\frac{S^2|\tilde{c_m}|^2}{2\sigma^2}\right\} \mu_{k,p}(\tilde{c}_m)\right. \\ & \quad \times \cosh\left(\frac{S \, \Re\{\tilde{c}_m\} \Re\left\{y^*(k) e^{j(2\pi k\vartheta + \phi)}\right\}}{\sigma^2} + \frac{L_{2p}(k)}{2}\right) \\ & \quad \left. \times \cosh\left(\frac{S \, \Im\{\tilde{c}_m\} \Im\left\{y^*(k) e^{j(2\pi k\vartheta + \phi)}\right\}}{\sigma^2} - \frac{L_{2p-1}(k)}{2}\right)\right]. \end{aligned} \tag{42}$$

Recalling that $\tilde{\mathcal{C}}_p = \{(2i-1)d_p + j(2n-1)d_p\}_{i,n=1}^{2^{p-1}}$, the sum over $\tilde{c}_m \in \tilde{\mathcal{C}}_p$ in (42) can be written as a double sum over the counters i and n after replacing $\tilde{c}_m$ by $(2i-1)d_p + j(2n-1)d_p$. Therefore, in order to factorize $D_{\boldsymbol{\alpha}}(k)$, the term $\mu_{k,p}(\tilde{c}_m) = \mu_{k,p}\big([2i-1]d_p + j[2n-1]d_p\big)$ must be factorized into two terms, one depending only on i and the other only on n. Here, we are actually dealing with the first $2p-2$ MSBs, $\bar{b}_1^m \bar{b}_2^m \bar{b}_3^m \cdots \bar{b}_{2p-3}^m \bar{b}_{2p-2}^m$. Hence, since the two remaining LSBs $\bar{b}_{2p-1}^m$ and $\bar{b}_{2p}^m$ (which are the same[8] for all $\tilde{c}_m \in \tilde{\mathcal{C}}_p$) are not involved in $\mu_{k,p}(\tilde{c}_m)$, they will be represented by "$\times\times$" in (8), i.e.,

$$\tilde{c}_m \longleftrightarrow \underbrace{\bar{b}_1^m \bar{b}_2^m \cdots \bar{b}_l^m \cdots \bar{b}_{2p-5}^m \bar{b}_{2p-4}^m}_{\bar{\boldsymbol{b}}_p^m} \bar{b}_{2p-3}^m \bar{b}_{2p-2}^m \times\times. \quad (43)$$

Furthermore, as highlighted in (43), it will shortly prove very useful to represent the first $2p-4$ MSBs by the shorthand notation $\bar{\boldsymbol{b}}_p^m$, i.e., $\bar{\boldsymbol{b}}_p^m \triangleq \bar{b}_1^m \bar{b}_2^m \cdots \bar{b}_l^m \cdots \bar{b}_{2p-5}^m \bar{b}_{2p-4}^m$. For more convenience, we will rather use the superscript (i,n) instead of m in (43) since $\tilde{c}_m = (2i-1)d_p + j(2n-1)d_p$. That is:

$$\tilde{c}_m \longleftrightarrow \bar{\boldsymbol{b}}_p^{(i,n)} \bar{b}_{2p-3}^{(i,n)} \bar{b}_{2p-2}^{(i,n)} \times\times. \quad (44)$$

Using this notation, all the points of the top-right quadrant of the obtained 2^{2p}-QAM constellation are graphically represented in Fig. 2 (on the top of the next page) where the bits $\bar{b}_{2p-3}^{(i,n)}$ and $\bar{b}_{2p-2}^{(i,n)}$ are being assigned their true values (in red color). Each symbol $\tilde{c}_m$ in $\tilde{\mathcal{C}}_p$ which has current coordinates $\big([2i-1]d_p\,, [2n-1]d_p\big)$ in the Cartesian coordinate system (CCS) of the considered 2^{2p}-QAM constellation ($x-$ axis and $y-$ axis in Fig. 2) already has some other old coordinates, $\big([2i'-1]d_p\,, [2n'-1]d_p\big)$, in the CCS associated to the original $2^{2(p-1)}$-QAM constellation ($x'-$ axis and $y'-$ axis in Fig. 2), associated with a symbol $c_{m'} = (2i'-1)d_p + j(2n'-1)d_p$ in $\mathcal{C}_{p-1}$. By inspecting both CCSs in Fig. 2, it can be shown that $c_{m'}$ can be expressed in terms of either (i',n') or (i,n) as follows:

$$\begin{aligned} c_{m'} &= (2i'-1)d_p + j(2n'-1)d_p, \\ &= (2i-1-2^{p-1})d_p + j(2n-1-2^{p-1})d_p. \end{aligned} \quad (45)$$

Moreover, since the first $2p-2$ MSBs of each symbol $\tilde{c}_m \in \tilde{\mathcal{C}}_p$ are obtained — during "*step 1*" — from the whole bit sequence of the symbol $c_{m'}$ (associated to it in the original $2^{2(p-1)}$-QAM constellation), we readily have the following result:

$$c_{m'} \longleftrightarrow \bar{\boldsymbol{b}}_p^{(i,n)} \bar{b}_{2p-3}^{(i,n)} \bar{b}_{2p-2}^{(i,n)}. \quad (46)$$

On the other hand, we recall the same decomposition $\mathcal{C}_{p-1} = \tilde{\mathcal{C}}_{p-1} \cup (-\tilde{\mathcal{C}}_{p-1}) \cup \tilde{\mathcal{C}}_{p-1}^* \cup (-\tilde{\mathcal{C}}_{p-1}^*)$ for the original $2^{2(p-1)}$-QAM constellation where $\tilde{\mathcal{C}}_{p-1}$ denotes its top-right quadrant. Then, for some $\tilde{c}_{m'} \in \tilde{\mathcal{C}}_{p-1}$, we have $c_{m'} \in \{\tilde{c}_{m'}, -\tilde{c}_{m'}, \tilde{c}_{m'}^*, -\tilde{c}_{m'}^*\}$. In turn, the symbols $c_{m'}$ themselves are obtained from a previous Gray-coded $2^{2(p-2)}$-QAM constellation by applying the same recursive procedure. Therefore, due to the symmetries of "*step 2*", it follows that $\tilde{c}_{m'}, -\tilde{c}_{m'}, \tilde{c}_{m'}^*$, and $-\tilde{c}_{m'}^*$ have the same $2p-4$ MSBs (which are represented by $\bar{\boldsymbol{b}}_p^{(i,n)}$). Consequently, according to the definition in (34), we have

$$\mu_{k,p-1}(\tilde{c}_{m'}) = \prod_{l=1}^{2(p-1)-2} e^{(2\bar{b}_l^{(i,n)}-1)\frac{L_l(k)}{2}}, \quad \forall\, \tilde{c}_{m'} \in \tilde{\mathcal{C}}_{p-1}$$

thereby yielding the following recursive property:

$$\begin{aligned} \mu_{k,p}(\tilde{c}_m) = \mu_{k,p-1}(\tilde{c}_{m'}) &\exp\left\{(2\bar{b}_{2p-3}^{(i,n)}-1)L_{2p-3}(k)/2\right\} \\ &\times \exp\left\{(2\bar{b}_{2p-2}^{(i,n)}-1)L_{2p-2}(k)/2\right\}. \end{aligned} \quad (47)$$

Actually, one needs to express the bits $\bar{b}_{2p-3}^{(i,n)}$ and $\bar{b}_{2p-2}^{(i,n)}$ explicitly as one function of i or n only and vice-versa, respectively, if $\mu_{k,p}(\tilde{c}_m)$ is to be factorized in terms of these two counters separately. Using $\lfloor x \rfloor$ to denote the floor function which returns the largest integer which is smaller than or equal to x, the following lemma finds this useful decomposition:

Lemma 1: $\forall\, i,n = 1,2,\ldots,2^{p-1}$, the two bits $\bar{b}_{2p-2}^{(i,n)}$ and $\bar{b}_{2p-3}^{(i,n)}$ are expressed as:

$$\bar{b}_{2p-2}^{(i,n)} = \left\lfloor \frac{i-1}{2^{p-2}} \right\rfloor \quad \text{and} \quad \bar{b}_{2p-3}^{(i,n)} = \left\lfloor \frac{n-1}{2^{p-2}} \right\rfloor. \quad (48)$$

Proof: See Appendix A.

Notice from (48) that $\bar{b}_{2p-2}^{(i,n)}$ and $\bar{b}_{2p-3}^{(i,n)}$ depend each on only one counter (either i or n). Actually, a more general and much useful result can be stated here:

1) Assertion: all the odd-position bits, $\{\bar{b}_{2l-1}^{(i,n)}\}_{l=1}^{p}$, are function of n only and all the even-position bits, $\{\bar{b}_{2l}^{(i,n)}\}_{l=1}^{p}$, are function of i only. This is a direct consequence of the following *lemma*:

Lemma 2: the obtained 2^{2p}-QAM Gray-coded constellation has the following property:

- The odd-position bits, $\bar{b}_{2l-1}^{(i,n)}$, do not change by scanning each *horizontal* line of constellation points.
- The even-position bits, $\bar{b}_{2l}^{(i,n)}$, do not change by scanning each *vertical* line of constellation points.

Proof: this property is trivially verified for the *initial* QPSK constellation depicted in Fig. 1. Now, assume that it is true at order $p-1$ (i.e., the previous $2^{2(p-1)}$-QAM constellation). Then, at order p, this property is automatically verified for the first $2p-2$ bits of all the obtained symbols. This is because the latter are obtained by placing the $2^{2(p-1)}$-QAM constellation as is in the top-right quadrant, $\tilde{\mathcal{C}}_p$, and the other quadrants are obtained via the three symmetries of "*step 2*". Moreover, since the basic QPSK constellation (from which the remaining two bits are copied) verifies the underlying property, the latter becomes true for all the bits of the obtained constellation points.

In a nutshell, the fact that odd-position bits, $\bar{b}_{2l-1}^{(i,n)}$, do not change for each horizontal line means that they do not change by varying the symbols' abscissa, $(2i-1)d_p$, or equivalently by changing the counter i. Therefore, $\{\bar{b}_{2l-1}^{(i,n)}\}_{l=1}^{p}$ are function of n only. The same reasons reveal that the even-position bits, $\{\bar{b}_{2l}^{(i,n)}\}_{l=1}^{p}$, are function of i only. This completes the proof of the assertion stated just before *Lemma 2*. As a consequence, we will from now on drop the vanishing counter from each group of bits and denote the latter, respectively, as $\bar{b}_{2l-1}^{(n)}$ and $\bar{b}_{2l}^{(i)}$ for $l = 1,2,\ldots,p$.

[8]The values of these two LSBs are defined according to the top-right quadrant of the basic Gray-coded QPSK constellation used in "*step 3*" during the recursive construction procedure. For instance, in the example depicted in Fig. 1, they will be "$\times\times = 11$".

Now, using the result in *Lemma 1* and the recursive property in (47), we show in Appendix B the following theorem:

Theorem 1: for any $p \geq 2$, $\mu_{k,p}(\tilde{c}_m)$ can be factorized into two independent terms each of which depends solely on one of the two counters i and n as follows:

$$\mu_{k,p}(\tilde{c}_m) = \theta_{k,2p}(i)\theta_{k,2p-1}(n), \tag{49}$$

where $\theta_{k,2p}(i)$ and $\theta_{k,2p-1}(n)$ are expressed as:

$$\theta_{k,2p}(i) \triangleq \prod_{l=1}^{p-1} e^{(2\bar{b}_{2l}^{(i)}-1)\frac{L_{2l}(k)}{2}} \tag{50}$$

$$\theta_{k,2p-1}(n) \triangleq \prod_{l=1}^{p-1} e^{(2\bar{b}_{2l-1}^{(n)}-1)\frac{L_{2l-1}(k)}{2}}. \tag{51}$$

Moreover, $\theta_{k,2p}(i)$ and $\theta_{k,2p-1}(n)$ can be computed recursively, from lower-order constellations, for any $p \geq 2$ as follows:

$$\theta_{k,2p}(i) = \theta_{k,2p-2}\left(\frac{|2i-1-2^{p-1}|+1}{2}\right) \times \exp\left\{\left(2\left\lfloor\frac{i-1}{2^{p-2}}\right\rfloor - 1\right)\frac{L_{2p-2}(k)}{2}\right\}, \tag{52}$$

$$\theta_{k,2p-1}(n) = \theta_{k,2p-3}\left(\frac{|2n-1-2^{p-1}|+1}{2}\right) \times \exp\left\{\left(2\left\lfloor\frac{n-1}{2^{p-2}}\right\rfloor - 1\right)\frac{L_{2p-3}(k)}{2}\right\}. \tag{53}$$

Proof: see Appendix B.

Note here that the initialization for (52) and (53) is simply given by $\theta_{k,2}(1) = \theta_{k,1}(1) = 1$. This is because we have extended the definition of $\mu_{k,p}(.)$ for $p = 1$ (i.e., QPSK constellations) to be $\mu_{k,1}(c_m) = 1 \ \forall \ c_m \in \mathcal{C}_1$ [just after (35)]. Therefore, denoting the single symbol in $\tilde{\mathcal{C}}_1$ as $\tilde{c}$, one can write $\mu_{k,1}(\tilde{c}) = \theta_{k,2}(1)\theta_{k,1}(1)$ as in (49) with $\theta_{k,2}(1) = \theta_{k,1}(1) = 1$. Plugging (49) in (42) and using the fact that $\tilde{\mathcal{C}}_p = \{(2i-1)d_p + j(2n-1)d_p\}_{i,n=1,2,\ldots,2^{p-1}}$, the term $D_{\boldsymbol{\alpha}}(k)$ is rewritten as follows:

$$D_{\boldsymbol{\alpha}}(k) = 4\beta_k \sum_{i=1}^{2^{p-1}}\sum_{n=1}^{2^{p-1}}\left[\exp\left\{-\frac{S^2((2i-1)^2+(2n-1)^2)d_p^2}{2\sigma^2}\right\} \theta_{k,2p}(i)\cosh\left(\frac{S(2i-1)d_p u(k)}{\sigma^2}+\frac{L_{2p}(k)}{2}\right) \times \theta_{k,2p-1}(n)\cosh\left(\frac{S(2n-1)d_p v(k)}{\sigma^2}-\frac{L_{2p-1}(k)}{2}\right)\right], \tag{54}$$

where $u(k)$ and $v(k)$ are defined as $u(k) = \Re\left\{y^*(k)e^{j(2\pi k\vartheta+\phi)}\right\}$ and $v(k) = \Im\left\{y^*(k)e^{j(2\pi k\vartheta+\phi)}\right\}$. Finally, splitting the two sums, it can be shown that $D_{\boldsymbol{\alpha}}(k)$ factorizes as follows:

$$D_{\boldsymbol{\alpha}}(k) = 4\beta_k \ F_{2p,\boldsymbol{\alpha}}(u(k)) \times F_{2p-1,\boldsymbol{\alpha}}(v(k)), \tag{55}$$

where $F_{q,\boldsymbol{\alpha}}(.)$ is given by:

$$F_{q,\boldsymbol{\alpha}}(x) = \sum_{i=1}^{2^{p-1}} \theta_{k,q}(i)\exp\left\{-\frac{S^2(2i-1)^2d_p^2}{2\sigma^2}\right\} \times \cosh\left(\frac{(2i-1)d_pSx}{\sigma^2}+(-1)^q\frac{L_q(k)}{2}\right), \tag{56}$$

and where, depending on the context, the counter q is used from now on to refer to $2p$ or $2p-1$. The factorization of $D_{\boldsymbol{\alpha}}(k)$ in (55) will prove very useful in deriving the analytical expressions of the considered stochastic CRLBs. In fact, by injecting (55) back into (28), the LLF for any square-QAM constellation (after discarding all the constant terms) is linearized as follows:

$$L_{\boldsymbol{y}}(\boldsymbol{\alpha}) = -K\ln(2\pi\sigma^2) - \frac{1}{2\sigma^2}\sum_{k=0}^{K-1}\left(I(k)^2+Q(k)^2\right) + \sum_{k=0}^{K-1}\ln\left(F_{2p,\boldsymbol{\alpha}}(u(k))\right) + \sum_{k=0}^{K-1}\ln\left(F_{2p-1,\boldsymbol{\alpha}}(v(k))\right), \tag{57}$$

involving thereby the sum of two analogous terms (the two last sums). Now, we further show that U_k and V_k [whose realizations are $u(k)$ and $v(k)$, respectively] are two independent random variables (RVs) which are *almost* identically distributed (i.e., their pdfs have the same structure, but are parameterized differently). In fact, injecting (55) in (26) and using the fact that $I(k)^2+Q(k)^2 = u(k)^2+v(k)^2$, it can be shown that $p[y(k);\boldsymbol{\alpha}]$ factorizes as follows:

$$p[y(k);\boldsymbol{\alpha}] = p[u(k);\boldsymbol{\alpha}]p[v(k);\boldsymbol{\alpha}], \tag{58}$$

where

$$p[u(k);\boldsymbol{\alpha}] = \frac{2\beta_{k,2p}}{\sqrt{2\pi\sigma^2}}\exp\left\{-\frac{u(k)^2}{2\sigma^2}\right\}F_{2p,\boldsymbol{\alpha}}(u(k)), \tag{59}$$

$$p[v(k);\boldsymbol{\alpha}] = \frac{2\beta_{k,2p-1}}{\sqrt{2\pi\sigma^2}}\exp\left\{-\frac{v(k)^2}{2\sigma^2}\right\}F_{2p-1,\boldsymbol{\alpha}}(v(k)), \tag{60}$$

with

$$\beta_{k,2p} = \prod_{l=1}^{p}\frac{1}{2\cosh\left(\frac{L_{2l}(k)}{2}\right)}, \ \beta_{k,2p-1} = \prod_{l=1}^{p}\frac{1}{2\cosh\left(\frac{L_{2l-1}(k)}{2}\right)}.$$

Moreover, we have $p[u(k),v(k);\boldsymbol{\alpha}] = p[y(k)^*e^{j(2\pi k\vartheta+\phi)};\boldsymbol{\alpha}]$ since $u(k)$ and $v(k)$ are indeed the real and imaginary parts of $y(k)^*e^{j(2\pi k\vartheta+\phi)}$. Then, since $e^{j(2\pi k\vartheta+\phi)}$ is assumed to be deterministic, we have $p[y(k)^*e^{j(2\pi k\vartheta+\phi)};\boldsymbol{\alpha}] = p[y(k);\boldsymbol{\alpha}]$. Therefore, using (58), we obtain:

$$p[u(k),v(k);\boldsymbol{\alpha}] = p[u(k);\boldsymbol{\alpha}]p[v(k);\boldsymbol{\alpha}], \tag{61}$$

meaning that U_k and V_k are two independent RVs *almost* identically distributed according to (59) and (60), since their joint distribution above is the product of their two separate distributions.

IV. Derivation of the CA CRLBs

In Section IV-A, we will develop the analytical expressions for the CA CRLBs of SNR estimates from coded BPSK-, MSK-

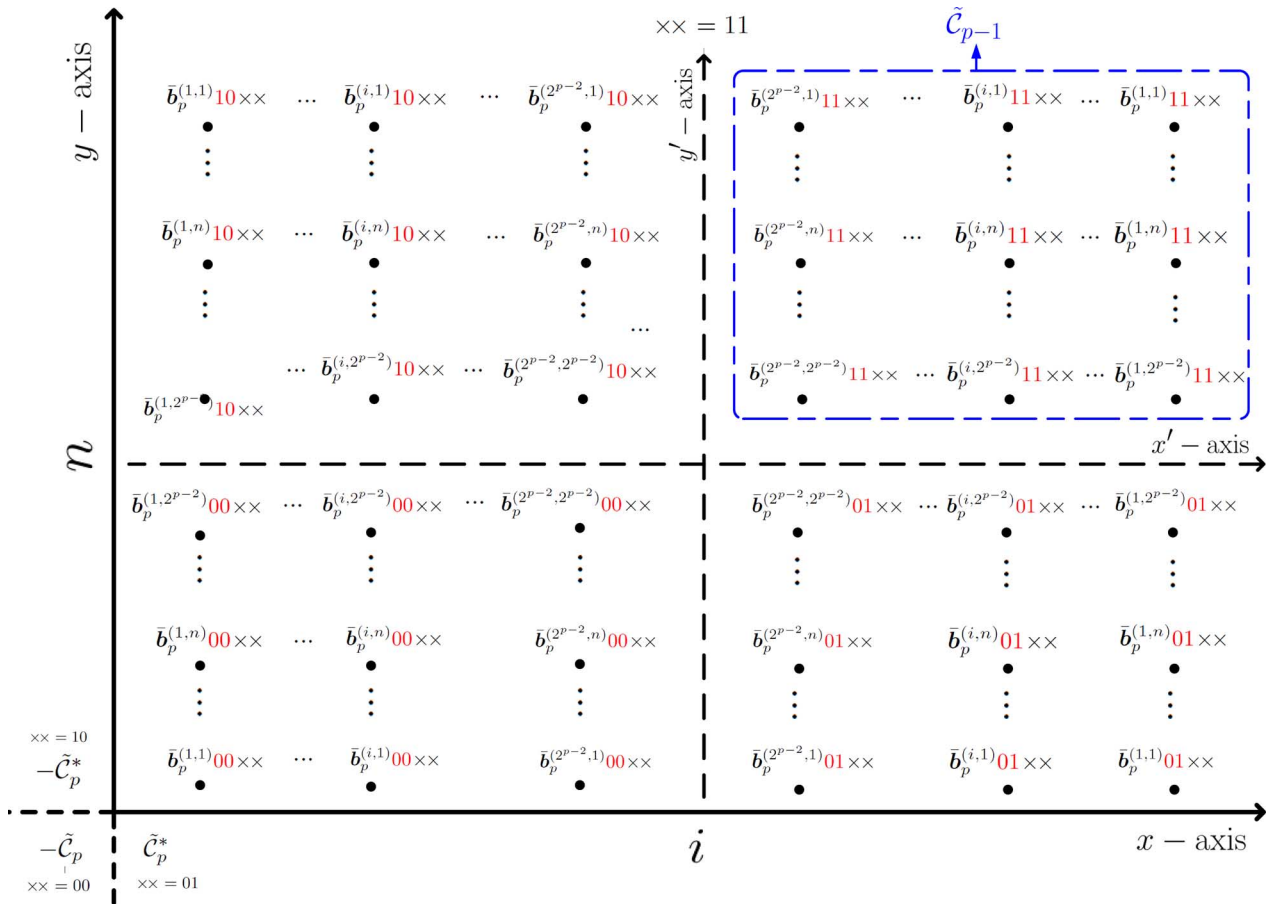

Fig. 2. General recursive construction of Gray-coded square-QAM constellations from $2^{2(p-1)}$-QAM to 2^{2p}-QAM.

and arbitrary square-QAM-modulated signals. For the sole purpose of their validation, we derive in Section IV-B their empirical counterparts (a set of valuable standalone would-have-been contribution if derivation of the analytical ones were not all made possible here, cf. Section I).

A. Derivation of the Analytical CRLBs

We begin first by deriving the FIM elements using the LLFs' expressions obtained in the previous section. We consider the case of square-QAM-modulated signals since it is the most general and tedious one. Similar derivations can be applied in the cases of BPSK-, MSK- and QPSK-modulated-signals to obtain the corresponding FIM elements. Due to space limitations also, we will provide the derivations details only for the first FIM element since the other ones can be obtained in the same way. Starting from (57), we readily have the following result:

$$\mathrm{E}_{\boldsymbol{y}}\left\{\frac{\partial^2 \ln(p[\boldsymbol{y};\boldsymbol{\alpha}])}{\partial S^2}\right\} = \sum_{k=0}^{K-1} \mathrm{E}\left\{\frac{\partial^2 \ln(F_{2p,\boldsymbol{\alpha}}(u(k)))}{\partial S^2}\right\} + \sum_{k=0}^{K-1} \mathrm{E}\left\{\frac{\partial^2 \ln(F_{2p-1,\boldsymbol{\alpha}}(v(k)))}{\partial S^2}\right\}. \quad (62)$$

As mentioned previously, the two terms in the right-hand side of (62) are analogous and they can be derived in the same way, especially because the RVs $u(k)$ and $v(k)$ are *almost* identically distributed. Thus, for ease of notations, we will henceforth use $z_q(k)$ to refer to $u(k)$ when $q = 2p$ and to $v(k)$ when $q = 2p-1$, respectively. Using this generic notation and defining:

$$\dot{F}_{q,\boldsymbol{\alpha}}(z_q(k)) \triangleq \frac{\partial F_{q,\boldsymbol{\alpha}}(z_q(k))}{\partial S},$$
$$\ddot{F}_{q,\boldsymbol{\alpha}}(z_q(k)) \triangleq \frac{\partial^2 F_{q,\boldsymbol{\alpha}}(z_q(k))}{\partial S^2},$$

it can be shown that:

$$\mathrm{E}\left\{\frac{\partial^2 \ln(F_{q,\boldsymbol{\alpha}}(z_q(k)))}{\partial S^2}\right\} = \mathrm{E}\left\{\frac{\ddot{F}_{q,\boldsymbol{\alpha}}(z_q(k))}{F_{q,\boldsymbol{\alpha}}(z_q(k))}\right\} - \mathrm{E}\left\{\frac{\dot{F}_{q,\boldsymbol{\alpha}}(z_q(k))^2}{F_{q,\boldsymbol{\alpha}}(z_q(k))^2}\right\}.$$

The second expectation is obtained by integrating over the distribution of $z_q(k)$ obtained earlier in (59) and (60) for $q = 2p$ and $q = 2p-1$, respectively:

$$\begin{aligned}
&\mathrm{E}\left\{\frac{\dot{F}_{q,\boldsymbol{\alpha}}(z_q(k))^2}{F_{q,\boldsymbol{\alpha}}(z_q(k))^2}\right\} \\
&= \int_{-\infty}^{+\infty} \frac{\dot{F}_{q,\boldsymbol{\alpha}}(z_q(k))^2}{F_{q,\boldsymbol{\alpha}}(z_q(k))^2} p[z_q(k),\boldsymbol{\alpha}] dz_q(k) \\
&= \frac{2\beta_{k,q}}{\sqrt{2\pi\sigma^2}} \int_{-\infty}^{+\infty} \frac{\dot{F}_{q,\boldsymbol{\alpha}}(z_q(k))^2}{F_{\boldsymbol{\alpha}}(z_q(k))} e^{-\frac{z_q(k)^2}{2\sigma^2}} dz_q(k), \quad (63)
\end{aligned}$$

where the expression of the first derivative, $\dot{F}_{q,\boldsymbol{\alpha}}(z_q(k))$, is given by (106) in Appendix C. We further simplify (63) by changing $z_q(k)/\sigma$ by t and using $\rho = S^2/2\sigma^2$ to obtain:

$$\mathrm{E}\left\{\frac{\dot{F}_{q,\boldsymbol{\alpha}}(z_q(k))^2}{F_{q,\boldsymbol{\alpha}}(z_q(k))^2}\right\} = \frac{2\beta_{k,q}d_p^2}{\sigma^2}\Psi_{k,q}(\rho), \tag{64}$$

in which $\Psi_{k,q}(\rho)$ is defined as:

$$\Psi_{k,q}(\rho) \triangleq \frac{1}{\sqrt{2\pi}}\int_{-\infty}^{+\infty}\frac{\lambda_{k,q}(\rho,t)^2}{\delta_{k,q}(\rho,t)}e^{-\frac{t^2}{2}}dt, \tag{65}$$

where, by using $\omega_{k,q}(i) \triangleq \theta_{k,q}(i)\, e^{-(2i-1)^2 d_p^2\rho}$, the functions $\delta_{k,q}(.,.)$ and $\lambda_{k,q}(.,.)$ are, respectively, given by

$$\delta_{k,q}(\rho,t) = \sum_{i=1}^{2^{p-1}}\omega_{k,q}(i)\cosh\left(\sqrt{2\rho}(2i-1)d_p t + \frac{(-1)^q L_q(k)}{2}\right), \tag{66}$$

and (67), shown at the bottom of the page. Furthermore, after tedious algebraic manipulations, we show in Appendix C the following identity:

$$\mathrm{E}\left\{\frac{\ddot{F}_{q,\boldsymbol{\alpha}}(z_q(k))}{F_{q,\boldsymbol{\alpha}}(z_q(k))}\right\} = 0. \tag{68}$$

Therefore, by using $\alpha_{k,q} \triangleq 2\beta_{k,q}d_p^2\Psi_{k,q}(\rho)$ and injecting (64) for $q = 2p$ and $q = 2p-1$ in (62), it follows that:

$$\mathrm{E}_{\boldsymbol{y}}\left\{\frac{\partial^2 \ln(P[\boldsymbol{y};\boldsymbol{\alpha}])}{\partial S^2}\right\} = -\frac{1}{\sigma^2}\sum_{k=0}^{K-1}\Big[\alpha_{k,2p} + \alpha_{k,2p-1}\Big]. \tag{69}$$

Equivalent algebraic manipulations, which are omitted here for the sake of conciseness, lead to the following analytical expressions for the second FIM's diagonal element:

$$\mathrm{E}_{\boldsymbol{y}}\left\{\frac{\partial^2 \ln(P(\boldsymbol{y};\boldsymbol{\alpha}))}{\partial {\sigma^2}^2}\right\} = \frac{K}{\sigma^4} + \frac{1}{\sigma^4}\sum_{k=0}^{K-1}\Big[\nu_{k,2p} + \nu_{k,2p-1}\Big], \tag{70}$$

where $\nu_{k,q}$ (for $q = 2p$ or $2p-1$) is given by:

$$\nu_{k,q} = c_{4,q}^{(k)}\rho^2 + 2\rho\left(c_{2,q}^{(k)} - 2\beta_{k,q}d_p^2\Phi_{k,q}(\rho)\right) - c_{0,q}^{(k)}. \tag{71}$$

The coefficients $c_{l,q}^{(k)}$ are given by[9]:

$$c_{l,q}^{(k)} = 2\beta_{k,q}d_p^l\cosh\big(L_q(k)/2\big)\sum_{i=1}^{2^{p-1}}\theta_{k,q}(i)(2i-1)^l. \tag{72}$$

and the function $\Phi_{k,q}(.)$ is defined as:

$$\Phi_{k,q}(\rho) \triangleq \frac{1}{\sqrt{2\pi}}\int_{-\infty}^{+\infty}\frac{\gamma_{k,q}^2(\rho,t)}{\delta_{k,q}(\rho,t)}e^{-\frac{t^2}{2}}dt, \tag{73}$$

where $\gamma_{k,q}(.,.)$ is defined by (74) at the bottom of the page. Equivalent derivations also yield the following expression for the off-diagonal element of $\boldsymbol{I}(\boldsymbol{\alpha})$:

$$\mathrm{E}_{\boldsymbol{y}}\left\{\frac{\partial^2 \ln(P[\boldsymbol{y};\boldsymbol{\alpha}])}{\partial\sigma^2\partial S}\right\} = -\frac{S}{\sigma^4}\sum_{k=0}^{K-1}\Big[\eta_{k,2p} + \eta_{k,2p-1}\Big], \tag{75}$$

in which $\eta_{k,q} \triangleq c_{2,q}^{(k)} - 2d_p^2\ \beta_{k,q}\ \Omega_{k,q}(\rho)$ with the function $\Omega_{k,q}(.)$ being defined as:

$$\Omega_{k,q}(\rho) \triangleq \frac{1}{\sqrt{2\pi}}\int_{-\infty}^{+\infty}\frac{\gamma_q(\rho,t)\lambda_q(\rho,t)}{\delta_q(\rho,t)}e^{-\frac{t^2}{2}}dt. \tag{76}$$

Therefore, from (69), (70) and (75), the global FIM decomposes into the sum of elementary FIMs:

$$\boldsymbol{I}(\boldsymbol{\alpha}) = \sum_{k=0}^{K-1}\boldsymbol{I}_k(\boldsymbol{\alpha}), \tag{77}$$

where $\{\boldsymbol{I}_k(\boldsymbol{\alpha})\}_{k=0}^{K-1}$ is the FIM pertaining to the estimation of the SNR from the received sample $y(k)$ alone:

$$\boldsymbol{I}_k(\boldsymbol{\alpha}) = \frac{1}{\sigma^4}\begin{pmatrix}\sigma^2\big[\alpha_{k,2p} + \alpha_{k,2p-1}\big] & S\big[\eta_{k,2p} + \eta_{k,2p-1}\big] \\ S\big[\eta_{k,2p} + \eta_{k,2p-1}\big] & -\big[\nu_{k,2p} + \nu_{k,2p-1} + 1\big]\end{pmatrix}. \tag{78}$$

This general FIM expression in CA estimation corroborates the two traditional extreme cases of completely NDA and completely DA estimations. Indeed, in the former case, no *a priori* information about the bits is available at the receiver end and, therefore, $P[b_l^k = 1] = P[b_l^k = 0] = 1/2$ thereby yielding $L_l^{\mathrm{NDA}}(k) = 0$ for all l and k. In the latter case, however, the bits are *a priori* perfectly known and, therefore, at the receiver side we have either $\{P[b_l^k = 1] = 1 \text{ hence } P[b_l^k = 0] = 0\}$ or $\{P[b_l^k = 0] = 1 \text{ hence } P[b_l^k = 1] = 0\}$ and consequently

[9]For the specific case of $l = 0$, it can be further shown that $c_{0,q}^{(k)} = 1$.

$$\lambda_{k,q}(\rho,t) = \sum_{i=1}^{2^{p-1}}(2i-1)^2\omega_{k,q}(i)\left[t\sinh\left(\sqrt{2\rho}\,(2i-1)d_p t + \frac{(-1)^q L_q(k)}{2}\right) - d_p(2i-1)\sqrt{2\rho}\cosh\left(\sqrt{2\rho}(2i-1)d_p t + \frac{(-1)^q L_q(k)}{2}\right)\right]. \tag{67}$$

$$\gamma_{k,q}(\rho,t) = \sum_{i=1}^{2^{p-1}}(2i-1)^2\omega_{k,q}(i)\left[t\sinh\left(\sqrt{2\rho}\,(2i-1)d_p t + \frac{(-1)^q L_q(k)}{2}\right) - d_p(2i-1)\sqrt{\frac{\rho}{2}}\cosh\left(\sqrt{2\rho}(2i-1)d_p t + \frac{(-1)^q L_q(k)}{2}\right)\right]. \tag{74}$$

the LLRs verify $L_l^{\mathrm{DA}}(k) = \pm\infty$. By injecting $L_l^{\mathrm{NDA}}(k)$ and $L_l^{\mathrm{DA}}(k)$ in the entries of $\boldsymbol{I}_k(\boldsymbol{\alpha})$ and by recurring to some easy simplifications[10], one obtains exactly the same expressions for the FIMs developed recently in [29] in the traditional NDA and DA cases, respectively.

Now, since the inverse of any (2×2) matrix is directly obtained by swapping the two diagonal elements and negating the off-diagonal ones, it can be shown from (77) that:

$$\boldsymbol{I}(\boldsymbol{\alpha})^{-1} = \sum_{k=0}^{K-1} \frac{\det\{\boldsymbol{I}_k(\boldsymbol{\alpha})\}}{\det\{\boldsymbol{I}(\boldsymbol{\alpha})\}} \boldsymbol{I}_k(\boldsymbol{\alpha})^{-1}, \tag{79}$$

where $\det\{.\}$ returns the determinant of any square matrix. Finally, injecting (79) and (6) in (5), it can be shown that:

$$\mathrm{CRLB}(\rho) = \sum_{k=0}^{K-1} \omega(k)\, \mathrm{CRLB}_k(\rho), \quad [\mathrm{dB}^2] \tag{80}$$

where $\omega(k) \triangleq \det\{\boldsymbol{I}_k(\boldsymbol{\alpha})\} / \det\{\boldsymbol{I}(\boldsymbol{\alpha})\}$ and $\mathrm{CRLB}_k(\rho)$ is the elementary CRLB pertaining to the estimation of the SNR given the received sample $y(k)$ only. The higher the weighting coefficient, $\omega(k)$, the more $y(k)$ contributes to the overall performance limit. These coefficients are not equal since the received samples are not identically distributed in contrast to the NDA estimation scenario. Indeed, the latter yield identical elementary FIMs and equal weighting coefficients leading thereby to a factor $1/K$ in the overall CRLB as shown in [29]. Now, in order to explicitly express the CA CRLBs, one must use the overall FIM, $\boldsymbol{I}(\boldsymbol{\alpha})$, given by (77) [which obtained implicitly from (78)] and which is valid for both the *linear* and *decibels* [dB] scales. In particular, if one is using the *linear* scale, then the corresponding overall CA CRLB is obtained by injecting in (5) the second expression for the derivative of $g(\boldsymbol{\alpha})$ in (6) along with $\boldsymbol{I}(\boldsymbol{\alpha})$. After some algebraic manipulations, it can be shown that the overall CRLB for CA SNR estimates (in *linear scale*) of square QAM signals is given by (81) at the bottom of the page. If one is, however, using the [dB] scale, then by using the following identity which follows from both equalities in (6):

$$\underbrace{\frac{\partial g(\boldsymbol{\alpha})}{\partial \boldsymbol{\alpha}}}_{\text{in [dB] scale}} = \frac{10}{\ln(10)\rho} \underbrace{\frac{\partial g(\boldsymbol{\alpha})}{\partial \boldsymbol{\alpha}}}_{\text{in linear scale}}, \tag{82}$$

it can be directly shown from (5) that the CRLB for CA SNR estimates in the [dB] scale is directly deduced from the CA CRLB in the *linear* scale, given by (81) on the bottom of the page, as follows:

$$\underbrace{\mathrm{CRLB}(\rho)}_{\text{in [dB] scale}} [\mathrm{dB}^2] = \frac{100}{\ln(10)^2\rho^2} \underbrace{\mathrm{CRLB}(\rho)}_{\text{in linear scale}}. \tag{83}$$

[10]The details are omitted here due to lack of space.

Equivalent derivations lead to the following simple and common CRLB expression for both BPSK and MSK signals:

$$\mathrm{CRLB}(\rho) = \frac{100}{\ln^2(10)K\rho} \frac{\rho\big[H(\rho) - K\big] - 2K}{\big[1 + 2\rho\big]H(\rho) - K}, \quad [\mathrm{dB}^2] \tag{84}$$

where

$$H(\rho) = \frac{e^{-\rho}}{\sqrt{2\pi}} \sum_{k=0}^{K-1} \frac{h_k(\rho)}{\cosh\left(L(k)/2\right)}, \tag{85}$$

with

$$h_k(\rho) = \int_{-\infty}^{+\infty} \frac{t^2 e^{-\frac{t^2}{2}}}{\cosh\left(\sqrt{2\rho}t + L(k)/2\right)} dt. \tag{86}$$

Again, when $L(k) = 0$, it can be easily verified that (84) yields exactly the same expression for the NDA CRLB derived for the very first time over a decade ago in [27] for BPSK. For QPSK, the second to the only two cases addressed in that seminal work, the CRLB can be simply obtained as a special case of square-QAM with $p = 1$. Finally, it is worth mentioning that all the derivations steps included in this paper are valid for coded systems in general. Therefore, the CA SNR CRLBs derived here are valid for any coded system. They can be evaluated as far as the receiver decoder is able to produce soft estimates for the LLRs of the bits (since they are the only quantities needed to evaluate the CA CRLBs). Fortunately, owing to the turbo decoding principle, it was shown in [8] that the *extrinsic* information of the bits, which is delivered during the decoding process, is an accurate estimate of these LLRs. Therefore, the above CRLBs can also be evaluated for LDCP-coded systems, as well, when they are decoded using the turbo principal (i.e., MAP or BCJR decoder) since they also produce the *extrinsic* information during the decoding process.

B. Derivation of the Empirical CRLBs

In this subsection, we develop an empirical procedure that evaluates the considered CRLBs through extensive Monte-Carlo simulations. These empirical CRLBs, a set of valuable would-have-been contribution rendered at once obsolete with the analytical ones achieved above, are still derived here for the sole purpose of validating the new closed-form expressions. In fact, the CRLBs can be obtained alternatively from the symbols' *a posteriori* probabilities (APPs). We will also rely on another definition for the FIM elements which involves the partial first derivatives of the LLF instead of its second derivatives. In fact, as shown in [26], the FIM elements can be written in the following equivalent form:

$$\boldsymbol{I}_{i,j}(\boldsymbol{\alpha}) = \mathrm{E}\left\{ \frac{\partial \ln(p[\boldsymbol{y};\boldsymbol{\alpha}])}{\partial \alpha_i} \frac{\partial \ln(p[\boldsymbol{y};\boldsymbol{\alpha}])}{\partial \alpha_j} \right\} \tag{87}$$

$$\mathrm{CRLB}(\rho) = \frac{2\rho\left(K + \sum_{k=0}^{K-1}\Big[\nu_{k,2p}(\rho) + \nu_{k,2p-1}(\rho)\Big]\right) - \rho^2\left(\sum_{k=0}^{K-1}\Big[4\eta_{k,2p}(\rho) + 4\eta_{k,2p-1}(\rho) + \alpha_{k,2p}(\rho) + \alpha_{k,2p-1}(\rho)\Big]\right)}{\left(K + \sum_{k=0}^{K-1}\Big[\nu_{k,2p}(\rho) + \nu_{k,2p-1}(\rho)\Big]\right)\left(\sum_{k=0}^{K-1}\Big[\alpha_{k,2p}(\rho) + \alpha_{k,2p-1}(\rho)\Big]\right) - 2\rho\left(\sum_{k=0}^{K-1}\Big[\eta_{k,2p}(\rho) + \eta_{k,2p-1}(\rho)\Big]\right)^2}. \tag{81}$$

where

$$\ln(p[\boldsymbol{y};\boldsymbol{\alpha}]) = \ln\left(\sum_{l=1}^{M^K} P[\boldsymbol{x}=\boldsymbol{x}_l]p[\boldsymbol{y}\,|\boldsymbol{x}=\boldsymbol{x}_l;\boldsymbol{\alpha}]\right), \quad (88)$$

is another formulation for the LLF in which $\boldsymbol{x} = [x(0), x(1), \ldots, x(K-1)]$ is a vector that contains the *actual* sequence of transmitted symbols and $\{\boldsymbol{x}_l\}_{l=1}^{M^K}$ are all the *possible* sequences of coded symbols that $\boldsymbol{x}$ can take. Differentiating (88) with respect to α_i and using the fact that $\partial p[\boldsymbol{y}\,|\,\boldsymbol{x}=\boldsymbol{x}_l;\boldsymbol{\alpha}]/\partial\alpha_i = p[\boldsymbol{y}|\boldsymbol{x}=\boldsymbol{x}_l;\boldsymbol{\alpha}]\times\partial\ln(p[\boldsymbol{y}\,|\,\boldsymbol{x}=\boldsymbol{x}_l;\boldsymbol{\alpha}])/\partial\alpha_i$ lead to the following expression:

$$\frac{\partial\ln(p[\boldsymbol{y};\boldsymbol{\alpha}])}{\partial\alpha_i} = \sum_{l=1}^{M^K}\frac{P[\boldsymbol{x}=\boldsymbol{x}_l]p[\boldsymbol{y}\,|\boldsymbol{x}=\boldsymbol{x}_l;\boldsymbol{\alpha}]}{p[\boldsymbol{y};\boldsymbol{\alpha}]} \times\frac{\partial\ln\left(p[\boldsymbol{y}\,|\boldsymbol{x}=\boldsymbol{x}_l;\boldsymbol{\alpha}]\right)}{\partial\alpha_i}. \quad (89)$$

Then, owing to Bayes' formula:

$$\frac{P[\boldsymbol{x}=\boldsymbol{x}_l]p[\boldsymbol{y}\,|\boldsymbol{x}=\boldsymbol{x}_l;\boldsymbol{\alpha}]}{p[\boldsymbol{y};\boldsymbol{\alpha}]} = p[\boldsymbol{x}=\boldsymbol{x}_l\,|\boldsymbol{y};\boldsymbol{\alpha}], \quad (90)$$

it follows that the right-hand side of (89) is nothing but the following conditional expectation:

$$\frac{\partial\ln(p[\boldsymbol{y};\boldsymbol{\alpha}])}{\partial\alpha_i} = \mathrm{E}_{\boldsymbol{x}|\boldsymbol{y}}\left\{\frac{\partial\ln\left(p[\boldsymbol{y}\,|\boldsymbol{x};\boldsymbol{\alpha}]\right)}{\partial\alpha_i}\right\}. \quad (91)$$

Now, since $p[\boldsymbol{y}\,|\boldsymbol{x};\boldsymbol{\alpha}] = \prod_{k=0}^{K-1} p[y(k)\,|x(k);\boldsymbol{\alpha}]$, then it follows from (91) that:

$$\frac{\partial\ln(p[\boldsymbol{y};\boldsymbol{\alpha}])}{\partial S} = \sum_{k=0}^{K-1}\mathrm{E}_{x(k)|\boldsymbol{y}}\left\{\frac{\Re\{y^*(k)x(k)S_{\phi,\vartheta}\}}{S\sigma^2} - \frac{S|x(k)|^2}{\sigma^2}\right\},$$

$$\frac{\partial\ln(p[\boldsymbol{y};\boldsymbol{\alpha}])}{\partial\sigma^2} = -\frac{K}{\sigma^2} + \sum_{k=0}^{K-1}\mathrm{E}_{x(k)|\boldsymbol{y}}\left\{\frac{|y(k)-x(k)S_{\phi,\vartheta}|^2}{2\sigma^4}\right\}.$$

The last two expectations are computed empirically using the marginal APPs provided by the decoder. In fact, in turbo-coded systems, these marginal APPs are computed iteratively using the BCJR algorithm in the two SISO decoders, with exchange of extrinsic information at each iteration. When the coded bits (conditioned on $\boldsymbol{y}$) can be considered as independent (which is again a reasonable assumption due to the large-size interleaver), this iterative procedure yields the correct marginal APPs at steady state [45]. The required APPs of each transmitted symbol are simply the product of the APPs of the corresponding bits that are delivered by the turbo decoder. To evaluate the FIM elements, however, the expectation involved in (87) is performed through extensive Monte-Carlo simulations by generating a sufficiently large number (say L) of noisy received sequences. The statistical expectation is then approximated by an arithmetical mean using all the generated realizations, according to the following formula:

$$\mathrm{E}\{f(X)\} = \frac{1}{L}\sum_{l=1}^{L} f(x_l). \quad (92)$$

which is valid for any transformation $f(.)$ of a given random variable X with realizations $\{x_l\}_{l=1}^{L}$.

V. Simulation Results

In this section, we provide graphical representations of the newly derived CA SNR CRLBs for different modulation orders and different coding rates using $K = 207$ received samples. The encoder is composed of two identical RSCs concatenated in parallel with systematic rate $R_0 = 1/2$ both and generator polynomials (1,0,1,1) and (1,1,0,1), respectively. A large-size interleaver is placed between the two RSCs. The output of the turbo encoder is punctured in order to achieve the desired overall coding rate (R). For the tailing bits, the size of the RSC encoders memory is fixed to 4.

In order to evaluate the CA CRLBs, we used the direct expressions in (50) and (51) for $\theta_{k,2p}(i)$ and $\theta_{k,2p-1}(n)$, respectively. Moreover, in order to smooth the curves for the analytical CA CRLBs, the bounds are averaged over 10 Monte-Carlo realizations (at each SNR point). This is because the *extrinsic* information for each bit (used to approximate the corresponding LLR) depends on the specific observation (i.e., noise realization). Hence, the CA CRLB can be averaged over a very small number of Monte-Carlo realizations (e.g., 10) in order to obtain smooth curves. Moreover, in all the subsequent simulations, we plot the CRLB in [dB^2] for the SNR estimates in [dB] scale.

In Figs. 3 and 4, we plot both the analytical and empirical CA CRLBs for 16-QAM and 64-QAM signals, respectively, with two different coding rates (i.e., $R_1 = 0.3285 \approx \frac{1}{3}$ and $R_2 = 0.4892 \approx \frac{1}{2}$). First, we clearly observe from both figures a perfect fit between the analytical and empirical CRLBs, validating thereby our new analytical expressions in all the considered cases.

We see also from both figures that the CRLB for CA estimation is smaller than the CRLB for the NDA scenario. This highlights the potential estimation performance gain that could be achieved by leveraging the information about the transmitted bits that could be gathered during the decoding process. This is in contrast with the traditional NDA scheme where the SNR is estimated directly from the output of the matched filter. Even though the CA scheme performs to the CRLB limit nearly as well as the NDA scheme at low SNR, near 0 dB, it always offers a potential gain (over the latter) that sharply increases with the SNR increasing. For instance, by the SNR value, $\rho = 4$ dB, the CA CRLB for 16-QAM signals soon becomes almost 10 times smaller than the NDA CRLB. From this relatively small SNR threshold, the CA CRLB starts to reach the DA CRLB simply given by [27]:

$$\mathrm{CRLB}_{\mathrm{DA}}(\rho) = \frac{100}{K\ln^2(10)}\left(1+\frac{2}{\rho}\right). \ [\mathrm{dB}^2] \quad (93)$$

Therefore, over a wide range of practical SNRs and without relying on any pilot sequence, CA estimation could potentially turn out to be equivalent to DA estimation which relies on the perfect knowledge of all the bits (or equivalently the symbols). Figs. 3 and 4 also show clearly the effect of the coding rate, R, on the SNR estimation performance. Even though the CA CRLBs corresponding to the two considered rates ultimately coincide at moderate SNR levels, they exhibit a significant gap at lower SNR values. In fact, with smaller coding rates, more redundancy can potentially be provided by the turbo encoder and the bits could then be decoded more accurately. In this case, the

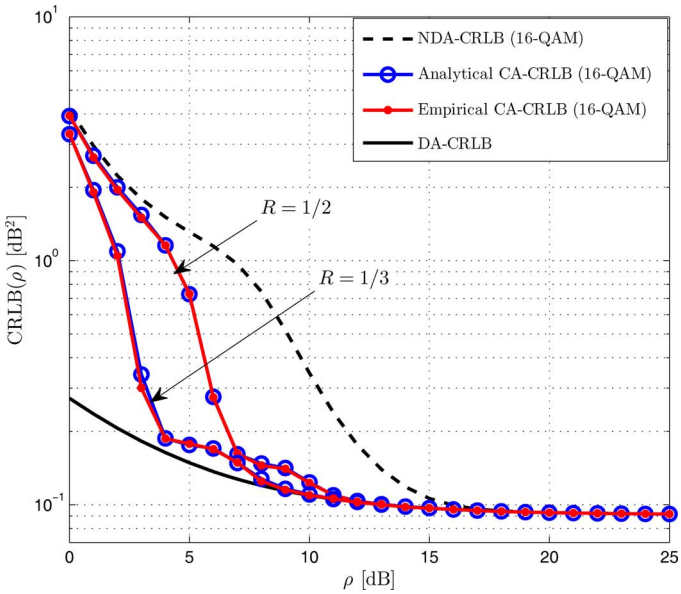

Fig. 3. CA vs. DA and NDA CRLBs [dB^2] for SNR estimation as function of the true SNR ρ [dB] with two different rates ($R = 1/3,\ 1/2$): 16-QAM.

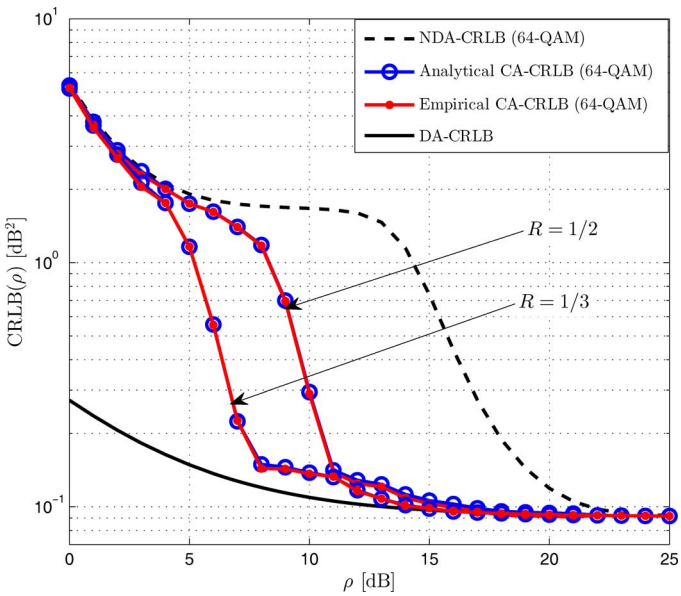

Fig. 4. CA vs. DA and NDA CRLBs [dB^2] for SNR estimation as function of the true SNR ρ [dB] with two different rates ($R = 1/3,\ 1/2$): 64-QAM.

extrinsic information, which is used to approximate the LLRs [8], [44], becomes increasingly high (in absolute value) and CA estimation becomes even closer in CRLB performance to DA estimation. By comparing Figs. 3 and 4 for a given code rate, we observe that the CA CRLBs increase with the modulation order and reach the DA CRLB at higher SNR thresholds as the constellation size increases.

In Fig. 5, we plot both the CA and DA CRLBs for BPSK-/MSK-modulated signals. In contrast to the higher-order modulations case, the gap between the NDA and DA CRLBs for both BPSK and MSK signals can be potentially bridged with CA estimation almost completely over the entire wide SNR range considered starting from around 0 dB.

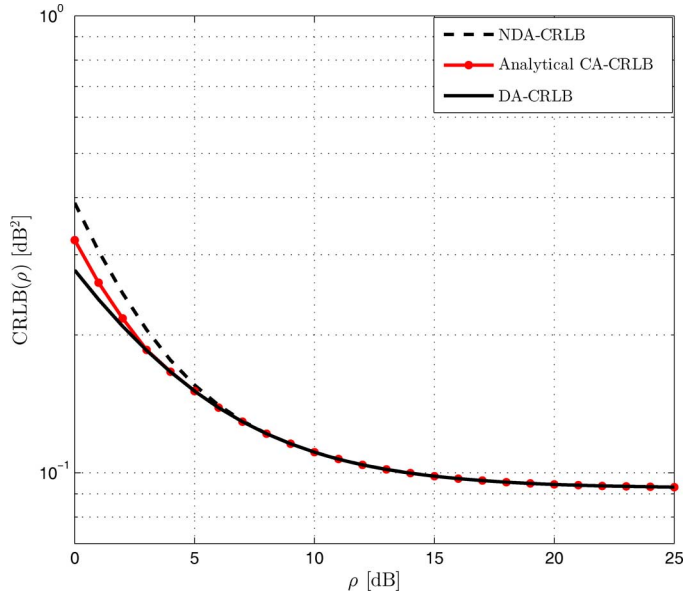

Fig. 5. CA vs. DA and NDA CRLBs [dB^2] for SNR estimation as function of the true SNR ρ [dB] for BPSK and MSK signals, $R = 1/2$.

Finally, it is worth mentioning that the SNR levels at which the CA CRLB touches the DA CRLB could be exploited in practice in order to predict the SNR thresholds at which a given turbo-coded system provides a decoding BER at which SNR estimation could nearly match the performance of the error-free decoding case.

VI. Conclusion

In this contribution, we established the analytical expressions for the CRLBs of SNR estimation from turbo-coded BPSK-, MSK-, and square-QAM transmissions. We have also verified for the sake of validation that our new analytical bounds perfectly match their empirical counterparts obtained here through extensive Monte-Carlo simulations. The new CA CRLBs are smaller than the NDA CRLBs thereby suggesting better SNR estimation potential when properly exploiting the SISO information about the transmitted bits that could be obtained from the decoder. Furthermore, the newly established CA CRLBs start to coincide with the DA CRLBs from relatively small SNR thresholds that further decrease with lower modulation orders and/or higher coding gains.

Appendix A
Proof of Lemma (48)

For better illustration, the two bits $\bar{b}_{2p-2}^{(i,n)}$ and $\bar{b}_{2p-3}^{(i,n)}$ are highlighted in red color in Fig. 2. We recall that they are added in "*step 3*" of the recursive construction from the lower-order $2^{2(p-1)}$-QAM constellation. Here, we focus only on the bit $\bar{b}_{2p-2}^{(i,n)}$ since the expression of $\bar{b}_{2p-3}^{(i,n)}$ can be obtained in the same way. We also consider the example of the basic QPSK constellation that is shown in Fig. 1. It can be seen that:

$$\bar{b}_{2p-2}^{(i,n)} = \begin{cases} 1 & \text{iff} \quad \Re\{c_{m'}\} > 0 \quad \text{(P1)} \\ 0 & \text{iff} \quad \Re\{c_{m'}\} < 0 \quad \text{(P2)}. \end{cases} \tag{94}$$

Then, according to (45), we have $(\mathrm{P1}) \Longleftrightarrow (2\mathrm{i}-1-2^{p-1}>0)$ and $(\mathrm{P2}) \Longleftrightarrow (2\mathrm{i}-1-2^{p-1}<0)$. We now show that:

$$(2i-1-2^{p-1}>0) \Longleftrightarrow \left\lfloor \frac{i-1}{2^{p-2}} \right\rfloor = 1, \tag{95}$$

$$(2i-1-2^{p-1}<0) \Longleftrightarrow \left\lfloor \frac{i-1}{2^{p-2}} \right\rfloor = 0. \tag{96}$$

Due to space limitations, we will only prove (95) since similar manipulations can easily prove (96).

- $\left(\overset{?}{\Longrightarrow}\right)$: On one hand, we have $2i-1-2^{p-1}>0 \Longrightarrow i > 2^{p-2}+1/2 > 2^{p-2}$. However, since we are comparing integers, this implies that $i \geq 2^{p-2}+1 \Longrightarrow i-1 \geq 2^{p-2}$ and, therefore, we have (a): $\frac{i-1}{2^{p-2}} \geq 1$. On the other hand, we have $i \leq 2^{p-1} \Longrightarrow i < 2^{p-1}+1$ and, therefore, we have (b): $\frac{i-1}{2^{p-2}} < 2^{p-1}/2^{p-2} = 2$. Thus, using (a) and (b), we obtain $1 \leq \frac{i-1}{2^{p-2}} < 2 \Longrightarrow \left\lfloor \frac{i-1}{2^{p-2}} \right\rfloor = 1$.
- $\left(\overset{?}{\Longleftarrow}\right)$: We have $\left\lfloor \frac{i-1}{2^{p-2}} \right\rfloor = 1 \Longrightarrow (i-1)/2^{p-2} \geq 1$ which implies $i \geq 2^{p-2}+1 \Longrightarrow i > 2^{p-2}+1/2$ and, therefore, $2i-1-2^{p-1}>0$, which completes the proof of (95).

Appendix B
Proof of Theorem 1

This theorem will be shown by mathematical induction for all $p \geq 2$. In fact, for $p=2$ (i.e., 16-QAM) it is seen from (34) that $\mu_{k,2}(\tilde{c}_m)$ involves the two first MSBs only. Hence, $\forall \tilde{c}_m \in \tilde{\mathcal{C}}_2$, we have:

$$\mu_{k,2}(\tilde{c}_m) = e^{(2\bar{b}_1^{(n)}-1)\frac{L_1(k)}{2}} e^{(2\bar{b}_2^{(i)}-1)\frac{L_2(k)}{2}} = \theta_{k,3}(n)\theta_{k,4}(i),$$

where $\theta_{k,4}(i)$ and $\theta_{k,3}(n)$ are given by $\theta_{k,4}(i) = e^{(2\bar{b}_2^{(i)}-1)\frac{L_2(k)}{2}}$ and $\theta_{k,3}(n) = e^{(2\bar{b}_1^{(n)}-1)\frac{L_1(k)}{2}}$. These are indeed special cases (for $p=2$) of (50) and (51), respectively. Thus, the theorem is trivially verified at order $p=2$. Now, assume that (49) is true at order $p-1$, $\forall\, p \geq 3$ (i.e., the $2^{2(p-1)}$-QAM). At order p (i.e., the 2^{2p}-QAM), we have from (47):

$$\mu_{k,p}(\tilde{c}_m) = \mu_{k,p-1}(\tilde{c}_{m'}) \exp\left\{(2\bar{b}_{2p-3}^{(n)}-1)L_{2p-3}(k)/2\right\} \times \exp\left\{(2\bar{b}_{2p-2}^{(i)}-1)L_{2p-2}(k)/2\right\}, \tag{97}$$

where $\mu_{k,p-1}(\tilde{c}_{m'})$ is defined over the $2^{2(p-1)}$-QAM constellation for which the property is assumed to hold true thereby implying:

$$\mu_{k,p-1}(\tilde{c}_{m'}) = \theta_{k,2(p-1)}(i')\theta_{k,2(p-1)-1}(n'), \tag{98}$$

in which i' and n' define the coordinates of $\tilde{c}_{m'}$ in the $2^{2(p-1)}$ constellation according to $\tilde{c}_{m'} = (2i'-1)d_p + j(2n'-1)d_p$. The expressions of $\theta_{k,2(p-1)}(i')$ and $\theta_{k,2(p-1)-1}(n')$ are given from (50) and (51) by:

$$\theta_{k,2(p-1)}(i') = \prod_{l=1}^{p-2} e^{(2\bar{b}_{2l}^{(i')}-1)\frac{L_{2l}(k)}{2}}, \tag{99}$$

$$\theta_{k,2(p-1)-1}(n') = \prod_{l=1}^{p-2} e^{(2\bar{b}_{2l-1}^{(n')}-1)\frac{L_{2l-1}(k)}{2}}. \tag{100}$$

Injecting (98) in (97) and rearranging the terms, one obtains:

$$\mu_{k,p}(\tilde{c}_m) = \left[\theta_{k,2(p-1)}(i')e^{(2\bar{b}_{2p-2}^{(i)}-1)\frac{L_{2p-2}(k)}{2}}\right] \times \left[\theta_{k,2(p-1)-1}(n')e^{(2\bar{b}_{2p-3}^{(n)}-1)\frac{L_{2p-3}(k)}{2}}\right]. \tag{101}$$

Recall that $\tilde{c}_{m'}$ lies in the top-right quadrant, $\tilde{\mathcal{C}}_{p-1}$, of the previous $2^{2(p-1)}$-QAM constellation whose CCS is defined by the x'– and y'–axes in Fig. 2. Recall also from the reasoning between (44) and (47) that the symbols $\tilde{c}_{m'}$ and $\tilde{c}_m$ have exactly the same $2p-4$ MSBs, i.e., $\bar{b}_{2l}^{(i')} = \bar{b}_{2l}^{(i)}$ and $\bar{b}_{2l-1}^{(n')} = \bar{b}_{2l-1}^{(n)}$ for $l = 1, 2, \ldots, p-2$. Using these results in (99) and (100), it follows that:

$$\theta_{k,2(p-1)}(i') = \prod_{l=1}^{p-2} e^{(2\bar{b}_{2l}^{(i)}-1)\frac{L_{2l}(k)}{2}}, \tag{102}$$

$$\theta_{k,2(p-1)-1}(n') = \prod_{l=1}^{p-2} e^{(2\bar{b}_{2l-1}^{(n)}-1)\frac{L_{2l-1}(k)}{2}}. \tag{103}$$

Hence, by making use of (102) along with (48), we obtain the result given by

$$\begin{aligned}\theta_{k,2(p-1)}(i')&e^{(2\bar{b}_{2p-2}^{(i)}-1)\frac{L_{2p-2}(k)}{2}} \\ &= \left(\prod_{l=1}^{p-2} e^{(2\bar{b}_{2l}^{(i)}-1)\frac{L_{2l}(k)}{2}}\right) e^{(2\bar{b}_{2p-2}^{(i)}-1)\frac{L_{2p-2}(k)}{2}} \\ &= \prod_{l=1}^{p-1} e^{(2\bar{b}_{2l}^{(i)}-1)\frac{L_{2l}(k)}{2}} = \theta_{k,2p}(i).\end{aligned} \tag{104}$$

in which the last equality follows immediately from the definition in (50). Using the same steps in (104), we show that:

$$\theta_{k,2(p-1)-1}(n')e^{(2\bar{b}_{2p-3}^{(n)}-1)\frac{L_{2p-3}(k)}{2}} = \theta_{k,2p-1}(n). \tag{105}$$

Finally, using (104) and (105) in (101) leads to $\mu_{k,p}(\tilde{c}_m) = \theta_{k,2p}(i)\theta_{k,2p-1}(n)$, meaning that the property is also true at order p and thus always true. This completes the proof of the first part of *Theorem 1*. The proof of its second part (recursive relations) follows immediately from (104) and (105). In fact, by using $\theta_{k,2p}(i) = \theta_{k,2(p-1)}(i')e^{(2\bar{b}_{2p-2}^{(i)}-1)\frac{L_{2p-2}(k)}{2}}$, (52) is a direct result of the fact that $i' = \frac{|2i-1-2^{p-1}|+1}{2}$ which is obtained from (45). The recursive relation in (53) is shown similarly by considering the counter n' and using (105).

Appendix C
Proof of (68)

We begin by developing the first and the second derivatives of $F_{q,\boldsymbol{\alpha}}(.)$ with respect to S as follows:

$$\begin{aligned}&\frac{\partial F_{q,\boldsymbol{\alpha}}(z_q(k))}{\partial S} \\ &= \sum_{i=1}^{2^{p-1}} \theta_{k,q}(i) e^{-\frac{(2i-1)^2 d_p^2 S^2}{2\sigma^2}} \\ &\times \left[\frac{(2i-1)d_p z_q(k)}{\sigma^2}\sinh\left(\frac{(2i-1)d_p S z_q(k)}{\sigma^2} + \frac{L_q(k)}{2}\right)\right. \\ &\left. -\frac{(2i-1)^2 d_p^2 S}{\sigma^2}\cosh\left(\frac{(2i-1)d_p S z_q(k)}{\sigma^2} + \frac{L_q(k)}{2}\right)\right].\end{aligned} \tag{106}$$

Then, by denoting $A_i = \sqrt{2\rho}(2i-1)d_p/\sigma$, we obtain:

$$\begin{aligned}
&\frac{\partial^2 F_{q,\boldsymbol{\alpha}}(z_q(k))}{\partial S^2} \\
&= \sum_{i=1}^{2^{p-1}} \theta_{k,q}(i) e^{-\frac{(2i-1)^2 d_p^2 S^2}{2\sigma^2}} \\
&\times \left[\frac{\left[(2i-1)d_p z_q(k)\right]^2}{\sigma^4} \cosh\left(A_i z_q(k) + \frac{L_q(k)}{2}\right) \right. \\
&- \frac{2(2i-1)^3 d_p^3 S z_q(k)}{\sigma^4} \sinh\left(A_i z_q(k) + \frac{L_q(k)}{2}\right) \\
&\left. + \left(\frac{(2i-1)^4 d_p^4 S^2)}{\sigma^4} - \frac{(2i-1)^2 d_p^2}{\sigma^2}\right) \cosh\left(A_i z_q(k) + \frac{L_q(k)}{2}\right) \right].
\end{aligned}$$

In order to find the expected value of $\ddot{F}_{q,\boldsymbol{\alpha}}(z_q(k))/F_{q,\boldsymbol{\alpha}}(z_q(k))$, we multiply it by the pdf of $z_q(k)$ and then integrate from $-\infty$ to $+\infty$. This yields the following result:

$$\begin{aligned}
&\mathrm{E}\left\{\frac{\ddot{F}_{q,\boldsymbol{\alpha}}(z_q(k))}{F_{q,\boldsymbol{\alpha}}(z_q(k))}\right\} \\
&= \frac{2\beta_{k,q}}{\sqrt{2\pi}\sigma} \sum_{i=1}^{2^{p-1}} \theta_{k,q}(i) e^{-\frac{(2i-1)^2 d_p^2 S^2}{2\sigma^2}} \\
&\quad \times \left[\frac{(2i-1)^2 d_p^2}{\sigma^4} \alpha_{\boldsymbol{\alpha}}(i) - \frac{2(2i-1)^3 d_p^3 S)}{\sigma^4} \gamma_{\boldsymbol{\alpha}}(i) \right. \\
&\quad \left. + \left(\frac{(2i-1)^4 d_p^4 S^2}{\sigma^4} - \frac{(2i-1)^2 d_p^2}{\sigma^2}\right) \lambda_{\boldsymbol{\alpha}}(k) \right], \quad (107)
\end{aligned}$$

where $\alpha_{\boldsymbol{\alpha}}(i)$, $\gamma_{\boldsymbol{\alpha}}(i)$, and $\lambda_{\boldsymbol{\alpha}}(i)$ are defined as:

$$\begin{aligned}
\alpha_{\boldsymbol{\alpha}}(i) &= \int_{-\infty}^{+\infty} z_q(k)^2 e^{-\frac{z_q(k)^2}{2\sigma^2}} \cosh\left(A_i z_q(k) + \frac{L_q(k)}{2}\right) dz_q(k), \\
\gamma_{\boldsymbol{\alpha}}(i) &= \int_{-\infty}^{+\infty} z_q(k) e^{-\frac{z_q(k)^2}{2\sigma^2}} \sinh\left(A_i z_q(k) + \frac{L_q(k)}{2}\right) dz_q(k), \\
\lambda_{\boldsymbol{\alpha}}(i) &= \int_{-\infty}^{+\infty} e^{-\frac{z_q(k)^2}{2\sigma^2}} \cosh\left(A_i z_q(k) + \frac{L_q(k)}{2}\right) dz_q(k).
\end{aligned}$$

To evaluate these integrals, we use following formulas [47, pp. 384–390] for any $a > 0$ and $b \in \mathbb{R}$:

$$\int_0^{+\infty} x^2 e^{-ax^2} \cosh(bx) dx = \frac{\pi(2a+b^2)}{8a^2\sqrt{a}} \exp\left\{\frac{b^2}{4a}\right\}, \quad (108)$$

$$\int_0^{+\infty} x e^{-ax^2} \sinh(bx) dx = \frac{b}{4a}\sqrt{\frac{\pi}{a}} \exp\left\{\frac{b^2}{4a}\right\}, \quad (109)$$

$$\int_0^{+\infty} e^{-ax^2} \cosh(bx) dx = \frac{1}{2}\sqrt{\frac{\pi}{a}} \exp\left\{\frac{b^2}{4a}\right\}. \quad (110)$$

Actually, by expanding the integrands and recognizing some odd and even functions, the integrals involved in the expressions of $\alpha_{\boldsymbol{\alpha}}(i)$, $\gamma_{\boldsymbol{\alpha}}(i)$, and $\lambda_{\boldsymbol{\alpha}}(i)$ reduce to those of (108)–(110). Thus, it can be shown that:

$$\begin{aligned}
\alpha_{\boldsymbol{\alpha}}(i) &= \cosh\left(\frac{L_q(k)}{2}\right) \sqrt{2\pi}(\sigma^3 + (2i-1)^2 d_p^2 \sigma S^2) e^{\frac{(2i-1)^2 d_p^2 S^2}{2\sigma^2}}, \\
\gamma_{\boldsymbol{\alpha}}(i) &= \cosh\left(\frac{L_q(k)}{2}\right) \sqrt{2\pi}(2i-1) d_p \sigma S e^{\frac{(2i-1)^2 d_p^2 S^2}{2\sigma^2}}, \\
\lambda_{\boldsymbol{\theta}}(k) &= \cosh\left(\frac{L_q(k)}{2}\right) \sqrt{2\pi}\sigma e^{\frac{(2i-1)^2 d_p^2 S^2}{2\sigma^2}}.
\end{aligned}$$

Injecting these results back into (107), we obtain the result given by (68).

REFERENCES

[1] S. Nanda, K. Balachandran, and S. Kumar, "Adaptation techniques in wireless packet data services," *IEEE Trans. Commun.*, vol. 38, no. 1, pp. 54–64, Jan. 2000.

[2] S. Talakoub and B. Shahrrava, "Turbo equalization with integrated SNR estimation," presented at the IEEE GLOBECOM, San Francisco, CA, USA, Nov. 2006.

[3] S. Talakoub and B. Shahrrava, "Turbo equalization with iterative online SNR estimation," in *Proc. IEEE WCNC*, New Orleans, LA, USA, Mar. 13–17, 2005, vol. 2, pp. 1097–1102.

[4] J. G. Proakis, *Digital Communications*. New York, NY, USA: McGraw-Hill, 2001.

[5] K. Balachandran, S. R. Kadaba, and S. Nanda, "Channel quality estimation and rate adaptation for cellular mobile radio," *IEEE J. Sel. Areas Commun.*, vol. 17, no. 7, pp. 1244–1256, Jul. 1999.

[6] C. Berrou and A. Glavieux, "Near optimum error correcting coding and decoding: Turbo codes," *IEEE Trans. Commun.*, vol. 44, no. 10, pp. 1261–1271, Oct. 1996.

[7] J. Hagenauer, "The turbo principle: Tutorial introduction and state of the art," in *Proc. Int. Symp. Turbo Codes Related Topics*, Brest, France, Sep. 1997, pp. 1–11.

[8] G. Colavolpe, G. Ferrari, and R. Raheli, "Extrinsic information in iterative decoding: A unified view," *IEEE Trans. Commun.*, vol. 49, no. 12, pp. 2088–2094, Dec. 2001.

[9] E. Dahlman, S. Parkvall, J. Sköld, and P. Beming, *3G Evolution: HSPA and LTE for Mobile Broadband*. Oxford, U.K.: Academic, 2007.

[10] M. A. Boujelben, F. Bellili, S. Affes, and A. Stéphenne, "SNR estimation over SIMO channels from linearly-modulated signals," *IEEE Trans. Signal Process.*, vol. 58, no. 12, pp. 6017–6028, Dec. 2010.

[11] A. Stéphenne, F. Bellili, and S. Affes, "Moment-based SNR estimation for SIMO wireless communication systems using arbitrary QAM," in *Proc. 41st Asilomar Conf. Signals, Syst., Comput.*, Pacific Grove, CA, USA, Nov. 4–7, 2007, pp. 601–605.

[12] M. A. Boujelben, F. Bellili, S. Affes, and A. Stéphenne, "EM algorithm for non-data-aided SNR estimation of linearly-modulated signals over SIMO channels," presented at the IEEE GLOBECOM, Honolulu, HI, USA, Dec. 2009.

[13] A. Stéphenne, F. Bellili, and S. Affes, "Moment-based SNR estimation over linearly-modulated wireless SIMO channels," *IEEE Trans. Wireless Commun.*, vol. 9, no. 2, pp. 714–722, Feb. 2010.

[14] M. A. Dangl and J. Lindner, "How to use a priori information of data symbols for SNR estimation," *IEEE Signal Process. Lett.*, vol. 13, no. 11, pp. 661–664, Nov. 2006.

[15] N. Wu, H. Wang, and J. M. Kuang, "Code-aided SNR estimation based on expectation maximisation algorithm," *Electron. Lett.*, vol. 44, no. 15, pp. 924–925, Jul. 2008.

[16] N. Wu, H. Wang, and J. M. Kuang, "Maximum likelihood signal-to-noise ratio estimation for coded linearly modulated signals," *IET Commun.*, vol. 4, pp. 265–271, 2010.

[17] M. Bergmann, W. Gappmair, H. Schlemmer, and O. Koudelka, "Code-aware joint estimation of carrier phase and SNR for linear modulation schemes," in *Proc. 5th Adv. Satellite Multimedia Syst. Conf.*, Cagliari, Italy, Sep. 2010, pp. 177–182.

[18] L. Bahl, J. Cocke, F. Jelinek, and J. Raviv, "Optimal decoding of linear codes for minimizing symbol error rate," *IEEE Trans. Inf. Theory*, vol. 20, no. 2, pp. 284–287, Mar. 1974.

[19] M. A. Khalighi, "Effect of mismatched SNR on the performance of log-MAP turbo detector," *IEEE Trans. Veh. Technol.*, vol. 52, no. 5, pp. 1386–1397, Sep. 2003.

[20] K. T. Shr and Y. H. Huang, "SNR estimation based on metric normalization frequency in Viterbi decoder," *IEEE Commun. Lett.*, vol. 15, no. 6, pp. 668–670, Jun. 2011.

[21] T. A. Summers and S. G. Wilson, "SNR mismatch and online estimation in turbo decoding," *IEEE Trans. Commun.*, vol. 46, no. 4, pp. 421–423, Apr. 1998.

[22] M. C. Reed and I. Asenstorfer, "A novel variance estimator for turbo-code decoding," presented at the ICT, Melbourne, Australia, Apr. 1997.

[23] S. Minying, L. Yuan, and S. Sumei, "Impact of SNR estimation error on turbo code with high-order modulation," presented at the IEEE VTC—Spring, Milan, Italy, May 2004.

[24] A. Worm, P. Hoeher, and N. Web, "Turbo-decoding without SNR estimation," *IEEE Commun. Lett.*, vol. 4, no. 6, pp. 193–195, Jun. 2000.

[25] *Evolved Universal Terrestrial Radio Access (E-UTRA); Physical Channels and Modulation, 3GPP TS 36.211, V8.2.0 (2008-03), Release 8*.
[26] S. M. Kay, *Fundamentals of Statistical Signal Processing*. Englewood Cliffs, NJ, USA: Prentice-Hall, 1993, vol. 1, Estimation Theory.
[27] N. S. Alagha, "Cramér-Rao bounds of SNR estimates for BPSK and QPSK modulated signals," *IEEE Commun. Lett.*, vol. 5, pp. 10–12, Jan. 2001.
[28] F. Bellili, A. Stéphenne, and S. Affes, "Cramér-Rao bounds for NDA SNR estimates of square QAM modulated signals," presented at the IEEE WCNC, Budapest, Hungary, Apr. 2009.
[29] F. Bellili, A. Stéphenne, and S. Affes, "Cramér-Rao lower bounds for NDA SNR estimates of square QAM modulated transmissions," *IEEE Trans. Commun.*, vol. 58, no. 11, pp. 3211–3218, Nov. 2010.
[30] J. Yang, B. Geller, and S. Bay, "Bayesian and hybrid Cramér-Rao bounds for the carrier recovery under dynamic phase uncertain channels," *IEEE Trans. Signal Process.*, vol. 59, no. 2, pp. 667–680, Feb. 2011.
[31] J. Yang, B. Geller, and A. Wei, "Approximate expressions for Cramér-Rao bounds of code aided QAM dynamical phase estimation," presented at the IEEE ICC, Dresden, Germany, Jun. 2009.
[32] S. Bay, B. Geller, A. Renaux, J. P. Barbot, and J. M. Brossier, "On the Hybrid Cramér Rao bound and its application to dynamical phase estimation," *IEEE Signal Process. Lett.*, vol. 15, pp. 453–456, May 2008.
[33] J. Yang, B. Geller, and A. Wei, "Bayesian and hybrid Cramer-Rao bounds for QAM dynamical phase estimation," presented at the IEEE ICASSP, Taipei, Taiwan, Apr. 2009.
[34] S. Bay, C. Herzet, J. M. Brossier, J. P. Barbot, and B. Geller, "Analytic and asymptotic analysis of bayesian Cramér-Rao bound for dynamical phase offset estimation," *IEEE Trans. Signal Process.*, vol. 56, no. 1, pp. 473–483, Jan. 2008.
[35] J. P. Delmas and H. Abeida, "Cramer-Rao bounds of DOA Estimates for BPSK and QPSK modulated signals," *IEEE Trans. Signal Process.*, vol. 54, no. 1, pp. 117–126, Jan. 2006.
[36] J. P. Delmas, "Closed-form expressions of the exact Cramer-Rao bound for parameter estimation of BPSK, MSK, or QPSK waveforms," *IEEE Signal Process. Lett.*, vol. 15, pp. 405–408, 2008.
[37] F. Rice, B. Cowley, B. Moran, and M. Rice, "Cramér-Rao lower bounds for QAM phase and frequency estimation," *IEEE Trans. Commun.*, vol. 49, no. 9, pp. 1582–1591, Sep. 2001.
[38] W. Gappmair, "Cramér-Rao lower bound for non-data-aided SNR estimation of linear modulation schemes," *IEEE Trans. Commun.*, vol. 56, no. 5, pp. 689–693, May 2008.
[39] I. Bergel and A. J. Weiss, "Cramér-Rao bound on timing recovery of linearly modulated signals with no ISI," *IEEE Trans. Commun.*, vol. 51, no. 4, pp. 634–640, Apr. 2003.
[40] F. Rice, M. Rice, and B. Cowley, "A new bound and algorithm for star 16-QAM carrier phase estimation," *IEEE Trans. Commun.*, vol. 51, no. 2, pp. 161–165, Feb. 2003.
[41] N. Noels, H. Wymeersch, H. Steendam, and M. Moeneclaey, "True Cramer-Rao bound for timing recovery from a bandlimited linearly modulated waveform with unknown carrier phase and frequency," *IEEE Trans. Commun.*, vol. 51, no. 3, pp. 473–483, Mar. 2004.
[42] W. Gappmair, R. Lopez-Valcarce, and C. Mosquera, "Joint NDA estimation of carrier frequency/phase and SNR for linearly modulated signal," *IEEE Signal Process. Lett.*, vol. 17, no. 5, pp. 517–520, May 2010.
[43] V. Lottici and M. Luise, "Embedding carrier phase recovery into iterative decoding of turbo-coded linear modulations," *IEEE Trans. Commun.*, vol. 52, no. 4, pp. 661–669, Apr. 2004.
[44] L. Zhang and A. Burr, "Iterative carrier phase recovery suited for turbo-coded systems," *IEEE Trans. Wireless Commun.*, vol. 3, no. 6, pp. 2267–2276, Nov. 2004.
[45] T. Richardson, "The geometry of turbo-decoding dynamics," *IEEE Trans. Inf. Theory*, vol. 46, no. 1, pp. 9–23, Jan. 2000.
[46] N. Noels, H. Steendam, and M. Moeneclaey, "The Cramér-Rao bound for phase estimation from coded linearly modulated signals," *IEEE Commun. Lett.*, vol. 7, no. 5, pp. 207–209, May 2003.
[47] A. Jeffrey and D. Zwillinger, *Tables of Integrals, Series, and Products*, 7th ed. New York, NY, USA: Academic, 2007.

Faouzi Bellili was born in Tunisia, on June 16, 1983. He received the Diplôme d'Ingénieur degree in signals and systems (with Hons.) from the Tunisia Polytechnic School in June 2007 and the M.Sc. degree, with the highest honor from the National Institute of Scientific Research (INRS-EMT), University of Quebec, Montreal, QC, Canada, in December 2009. He is currently working towards the Ph.D. degree at the INRS-EMT. He authored/co-authored over 40 peer-reviewed papers in reputable IEEE journals and conferences. His research focuses on statistical signal processing and array processing with an emphasis on parameters estimation for wireless communications. Mr. Bellili was selected by the INRS as its candidate for the 2009–2010 competition of the very prestigious Vanier Canada Graduate Scholarships program. He also received the Academic Gold Medal of the Governor General of Canada for the year 2009–2010 and the Excellence Grant of the Director General of INRS for the year 2009–2010. He also received the award of the best M.Sc. thesis of INRS-EMT for the year 2009–2010 and twice—for both the M.Sc. and Ph.D. programs—the National Grant of Excellence from the Tunisian Government. He was also rewarded in 2011 the Merit Scholarship for Foreign Students from the Ministère de l'Éducation, du Loisir et du Sport (MELS) of Québec, Canada. Mr. Bellili serves as a TPC member for the IEEE GLOBECOM conference and he acts regularly as a reviewer for many international scientific journals and conferences.

Achref Methenni was born in Dammam, Saudi Arabia, on November 19, 1987. He received the Diplôme d'Ingénieur degree in telecommunication from the Ecole Supérieure des Communications de Tunis-Sup'Com (Higher School of Communication of Tunis), Tunisia, in 2011 and the M.Sc. degree from the Institut National de la Recherche Scientifique-Energie, Matériaux, et Télécommunications (INRS-EMT), Université du Québec, Montréal, QC, Canada, in 2013. He is currently working toward the Ph.D. degree at INRS, Montreal, QC, Canada. His research activities include signal processing for Turbo-coded systems, and parameters estimation for wireless communications in general. Mr. Methenni received twice—for both the M.Sc. and Ph.D. programs—the National Grant of Excellence from the Tunisian Government.

Sofiène Affes (SM'04) received the Diplôme d'Ingénieur in telecommunications in 1992, and the Ph.D. degree with honors in signal processing in 1995, both from École Nationale Supérieure des Télécommunications (ENST), Paris, France. Since then, he was with INRS, Canada, as a Research Associate until 1997, an Assistant Professor until 2000, and Associate Professor until 2009. Currently he is Full Professor and Director of PERSWADE, a unique 4 million dollar research training program on wireless in Canada involving 27 faculty from 8 universities and 10 industrial partners. Dr. Affes has been twice the recipient of a Discovery Accelerator Supplement Award from NSERC, from 2008 to 2011, and from 2013 to 2016. From 2003 to 2013, he held a Canada Research Chair in Wireless Communications. In 2006, he served as General Co-Chair of IEEE VTC'2006-Fall, Montreal, Canada. In 2008 he received from the IEEE Vehicular Technology Society the IEEE VTC Chair Recognition Award for exemplary contributions to the success of IEEE VTC. He currently acts as an Associate Editor for the IEEE TRANSACTIONS ON COMMUNICATIONS and the Wiley *Journal on Wireless Communications & Mobile Computing*. From 2007 until 2013 and from 2010 until 2014, he has been an Associate Editor for the IEEE TRANSACTIONS ON WIRELESS COMMUNICATIONS and the IEEE TRANSACTIONS ON SIGNAL PROCESSING, respectively. He is serving now as General Co-Chair of IEEE ICUWB to be held in Montreal in fall 2015.